NASA Technical Memorandum 86276

Oil-Flow Study of a Space Shuttle Orbiter Tip-Fin Controller

Vernon T. Helms III

DECEMBER 1984

NASA

NASA Technical Memorandum 86276

Oil-Flow Study of a Space Shuttle Orbiter Tip-Fin Controller

Vernon T. Helms III
Langley Research Center
Hampton, Virginia

National Aeronautics
and Space Administration

**Scientific and Technical
Information Branch**

1984

Summary

Oil-flow patterns on a proposed tip-fin controller for the Space Shuttle orbiter are presented. These tests were conducted in air at Mach 10 for a free-stream Reynolds number of 1.13×10^6 at 20°, 30°, and 40°, angle of attack and sideslip angles of 0° and 2°. The effect of elevon deflections from −10° to 10° and of tip-fin control-surface deflections up to 40° on surface flow directions were investigated. It was determined that the tip-fin has very little effect on wing leeward surface flow patterns and that the most significant flow interactions occur on the outboard surface of the tip-fin.

Introduction

Technology for a second-generation space transportation system is currently being assessed at the NASA Langley Research Center. One of the major problem areas under investigation is yaw control for winged vehicles during entry at high angle of attack. On configurations such as the Space Shuttle, the rudder is ineffective as an aerodynamic control surface, because it is shielded from the flow until the final stages of entry when the vehicle is flying at low angle of attack. References 1 through 3 have shown that positive yaw control throughout the entry trajectory of a winged entry vehicle can be attained by omitting the vertical tail and adding small tip-fin controllers to the wing tips. Among the advantages cited in these reports for the tip-fin is a weight savings due to elimination of the vertical-tail structure and a reduced dependence on reaction control-system firings to provide control during entry. The Space Shuttle orbiter configuration has been used to study the control characteristics of tip-fins because of the broad wind-tunnel and flight aerodynamic data base available for comparison.

In addition to aerodynamic considerations, feasibility of the tip-fin concept depends on the thermal environment imposed upon the fin and the adjacent area of the wing upper surface. An investigation of tip-fin heating distributions on a Space Shuttle model using thermographic-phosphor and thin-film gauges is reported in reference 4. Nonuniform regions of locally enhanced heating of unexplained origins were observed on the tip-fin outboard surface at angles of attack to 40°, with and without tip-fin control-surface deflections. The purpose of the present study was to perform flow visualization, using the oil-flow technique, to assess the extent of flow interference effects on the wing and tip-fin which might lead to serious heating problems. This study was also intended to aid in the interpretation of observed heating distributions on the tip-fin outboard surface. An example of the correlation between surface flow directions and aerodynamic heating patterns on the tip-fin at $\alpha = 40°$ is included.

Symbols

h	local heat-transfer coefficient
h_{ref}	stagnation-point heat-transfer coefficient
M_∞	free-stream Mach number
Re_∞	free-stream Reynolds number based on model length
α	angle of attack, deg
β	sideslip angle, deg
δ_e	elevon deflection angle, deg
δ_{tf}	tip-fin deflection angle, deg

Apparatus and Methods

Tunnel

Tests were conducted in air using the Langley 31-Inch Mach 10 Tunnel (formerly the Langley Continuous-Flow Hypersonic Tunnel) operating in a blowdown mode. A description of this facility can be found in references 5 and 6. The model was rapidly injected into the flow through the tunnel sidewall after establishing steady flow conditions in the test section. The injection mechanism required less than 0.3 sec to place the model within the test core after first contact with the tunnel boundary layer. At the end of each run, which generally lasted from 20 to 30 sec, the model was retracted from the test section before shutting down the tunnel.

Model and Test Conditions

A 0.01-scale aluminum model of the Shuttle orbiter was modified for use in this study. Figure 1(a) is a photograph of the model with its tip-fins installed and the vertical tail removed. Details of the tip-fins are shown in figures 1(b) and 1(c). Tip-fin control-surface deflection angles of 0°, 20°, and 40° are shown in figure 1(b). The wings were equipped with changeable elevons to allow deflection-angle settings of −10°, 0°, and 10° (fig. 1(c)). Before performing the oil-flow tests, the model was coated with a high-temperature black paint and buffed lightly with No. 600 grit sandpaper and water to provide a smooth finish.

The oil-flow patterns were obtained at Mach 10 for a Reynolds number of 1.13×10^6, based on free-stream conditions and a model length of 1.075 ft. The angle of attack for the model was set at 20°, 30°, and 40°. The effect of a 2° sideslip angle on surface flow patterns was evaluated at each angle of attack for 0° deflection of the elevon and the tip-fin control surfaces. For $\beta = 0°$, tests were conducted with elevon deflection angles of −10°, 0°, and 10° using tip-fin control-surface deflections of 0°, 20°, and 40°.

Oil-Flow Technique

The oil used in this study was a mixture of Liquitex Artist Oil Color (Zinc Everwhite) and Dow Corning 200 Fluid silicone oil. Mixtures using fluids with viscosities of 10, 50, 100, and 200 centistokes (cs) were applied to different parts of the model. The low-viscosity 10-cs mixture was used on the wing leeward separated region and on the inboard surface of the tip-fin. The 50-cs mixture was applied to the wing leeward attached flow areas and to the outboard surface of the tip-fin at all angles of attack, and it was also used on the wing windward surface at 20° and 30° angle of attack. A 100-cs mixture was used on the wing windward surface and in combination with the 50-cs mixture on the outside tip-fin surface at all angles of attack. The high-viscosity 200-cs oil mixture was used only on the wing windward surface at 30° and 40° angle of attack. A light-to-moderate base coat of the clear 10-cs fluid was brushed onto the model surface, particularly in the low-shear areas, to act as a lubricant for the oil mixtures. Droplets of the mixtures were applied to the model by rapidly stroking the end of a small, stiff, mixture-laden brush with the forefinger to produce a thick array of white spots on the black surface. This procedure allowed satisfactory surface flow visualization to be obtained on both windward and leeward surfaces, as well as on the tip-fins, during the same wind-tunnel run. The model was removed from the wind-tunnel test section after each run to photograph the oil-flow patterns.

Results and Discussion

Figures 2 through 18 show oil-flow patterns, and one example of thermographic-phosphor heat-transfer results, obtained on the model wing and tip-fin over the range of test conditions previously described. Arrows indicating surface flow directions are included in some of these photographs to aid in the interpretation of the oil-flow patterns. A basic set of oil-flow patterns with no control-surface deflections is presented first. The changes induced in the basic patterns by a sideslip angle of 2° are then described. Flow patterns caused by elevon deflections of 10° and −10° are next compared with those for $\delta_e = 0°$, each for $\delta_{tf} = 0°$ and $\beta = 0°$. The last sets of figures detail tip-fin flow patterns with $\delta_{tf} = 20°$ and 40° for $\delta_e = 0°$ and no sideslip.

Oil-Flow Patterns for $\beta = 0°$, $\delta_e = 0°$, and $\delta_{tf} = 0°$

Figures 2 through 4 show oil-flow patterns for $\beta = 0°$, $\delta_e = 0°$, and $\delta_{tf} = 0°$ at $\alpha = 20°$, 30°, and 40°, respectively. Part (a) of each figure presents a full view of the wing leeward surface. As shown in figure 2(a), the separated region at $\alpha = 20°$ is dominated by reversed surface flow which sweeps forward toward the primary separation line. This flow originates at a line along the wing trailing edge which may be caused by reattachment of separated flow from forward locations on the wing or fuselage. It may also be possible that this line represents the reattachment of flow expanding around the wing trailing edge from the windward surface. A small pocket of reversed flow can be seen near the wing tip. This pocket also originates from flow reattachment close to the trailing edge and radiates in surface directions both inboard and outboard. This wing-tip flow structure is unrelated to the presence of the tip-fin. Figure 2(b) illustrates this point. It shows a previously unpublished photograph of wing leeward oil-flow patterns from a different test on another 0.01-scale Shuttle model without tip-fins at $M_\infty = 10$, $\alpha = 20°$, and $Re_\infty = 2.37 \times 10^6$. Although the higher Reynolds number produces a more extensive wing-tip reattachment in figure 2(b) than for the present test, the overall wing-tip pattern is still similar to that in figure 2(a). Also, a comparison of figures 2(a) and 2(b) shows that flow directions emanating from the outboard portion of the wing leading edge are nearly the same. The irregular trails overlapping the surface flow patterns, particularly in figure 2(b), are caused by excess oil running under the influence of gravity after the model was removed from the wind tunnel. Figure 2(c) shows that flow directions on the tip-fin appear to be nearly uniform over the entire inboard surface. Figure 2(d) indicates the presence of a reattachment line on the tip-fin outboard surface. The reattachment seems to form on the forward lower portion of the tip-fin, and it leaves the trailing edge near the 25-percent span location. This reattachment may be related to shedding of the wing-tip vortex. Figure 2(d) also shows that flow separation occurs over the aft lower portion of the tip-fin, where downward-moving flow from the reattachment line meets upward-moving flow that has come from the wing lower surface.

Surface flow patterns for $\alpha = 30°$ are presented in figure 3. Figure 3(a) shows oil-flow patterns on the left wing, and figures 3(b) and 3(c) are photographs of the tip-fin on the model's right wing. Photographs of both wings are used in this particular case to take advantage of the best oil-flow patterns obtained for each view. The wing leeward separated-region reattachment pattern in figure 3(a) occurs farther outboard than for $\alpha = 20°$. The outboard segment of the wing-tip reversed flow pattern reaches forward to the tip-fin aft area (fig. 3(b)). Flow from the wing-tip reversed pattern is forced up onto the inboard surface of the tip-fin and results in flow separation on its lower aft corner with indistinct traces of flow reattachment within the separated region. The reattachment line on the tip-fin outboard surface in figure 3(c) is more inclined relative to the plane of the wing than at the lower angle of attack. It leaves the tip-fin trailing edge near the 50-percent span location. The line of flow separation at the base of the tip-fin outer

surface has moved forward compared with the case of $\alpha = 20°$.

The primary wing separated-region reattachment pattern at $\alpha = 40°$ in figure 4(a) is much like that for $\alpha = 30°$, except that the wing area covered by the separated region has increased to the extent that outwardly directed flow from this pattern washes against the tip-fin inboard base region. The wing-tip reversed flow pattern has evolved to affect a large portion of the outer elevon. As at $\alpha = 30°$, the outboard segment of the reversed flow pattern reaches the tip-fin. Figure 4(b) shows how the outboard separated-region flow combines with wing-tip reversed flow to produce a large separation on the tip-fin inboard surface. A comparison of figures 3(b) and 4(b) illustrates the increased size of the tip-fin separation as angle of attack becomes larger. There are indications of reversed flow near the base of the tip-fin in figure 4(b) with a reattachment pattern at higher locations within the separated region. This is similar to the reattachment pattern on the tip-fin inboard surface observed at $\alpha = 30°$ in figure 3(b). The outboard tip-fin reattachment line for $\alpha = 40°$ in figure 4(c) leaves the trailing edge near the 75-percent span location. This represents a continuation of the increase in the reattachment line inclination as angle of attack becomes higher. Measurements from figures 2(c), 3(c), and 4(c) indicate that the angles of the reattachment line with respect to the model axis are 13°, 21°, and 30° for $\alpha = 20°$, 30°, and 40°, respectively. The reattachment line origin at $\alpha = 40°$ is close to the root of the tip-fin leading edge, which reflects an upward and forward movement compared with lower angles of attack. Flow separation on the lower portion of the tip-fin outer surface begins a short distance aft of the leading edge, and the associated area of attached flow from the wing lower surface is more extensive than for 20° or 30° angle of attack. Tip-fin inboard-surface flow directions not influenced by separation and reattachment effects are relatively insensitive to changes in angle of attack, whereas outboard-surface directions turn rapidly upward as angle of attack increases. (See figs. 2 through 4.)

Oil-Flow Patterns for $\beta = 2°$, $\delta_e = 0°$, and $\delta_{tf} = 0°$

Figures 5 through 7 show oil-flow results at $\alpha = 20°$, 30°, and 40°, respectively, for a sideslip angle of $\beta = 2°$ with no control-surface deflections. These photographs show the inboard and outboard surfaces of both the right and left tip-fins. The effects of sideslip can be seen by comparing these oil-flow patterns with the appropriate photographs in figures 2 through 4, where $\beta = 0°$. The "nose-left" rotation of the model for $\beta = 2°$ causes the right wing to turn more into the free stream than the left wing. Parts (a) and (b) of figures 5 through 7 show that one consequence of the sideslip angle is a smaller area of separated flow on the leeward surface of the right wing, which is indicated by the inboard movement of the primary separation line toward the slot between the elevons. Also, the reversed flow pattern near the wing tip is considerably more extensive on the right wing. As a result, the area of flow separation on the right tip-fin surface at $\alpha = 30°$ and 40° is much larger than on the left tip-fin. The size of the tip-fin inboard separated regions for $\beta = 0°$ (figs. 3(b) and 4(b)) is between that of the right and left tip-fin separations at $\beta = 2°$. The directions of attached flow on the inboard surfaces of both tip-fins are not noticeably different from those for $\beta = 0°$. The same is generally true of flow patterns on the outboard surfaces of the tip-fins. However, the inclination of the outboard reattachment line is approximately 1° lower on the right tip-fin and 1° higher on the left tip-fin than the values cited previously for each angle of attack.

Oil-Flow Patterns for $\beta = 0°$, $\delta_e = 10°$, and $\delta_{tf} = 0°$

Elevon deflections of 10° and −10° were found to have no effect on tip-fin flow patterns and very little influence on wing flow patterns in general. Representative oil-flow results illustrating this point are presented in figures 8 and 9 for $\alpha = 30°$. The only significant difference in wing leeward oil flows in figures 8(a) and 9(a) for deflected elevons compared with the case for $\delta_e = 0°$ in figure 3(a) is in the separated-flow reattachment patterns. Orientation of the reattachment line is spanwise for deflected elevons and longitudinal for $\delta_e = 0°$. The extent of flow separation on the lower aft inboard tip-fin surface is the same at $\delta_e = 10°$ and −10° in figures 8(b) and 9(b), respectively, and these photographs are indistinguishable from the one for $\alpha = 30°$ and $\delta_e = 0°$ in figure 3(b). Figures 8(c) and 9(c) also show identical oil flows on the tip-fin outer surface for the two elevon deflections.

Oil-Flow Patterns for $\beta = 0°$, $\delta_e = 0°$, and $\delta_{tf} = 20°$

An outward deflection of 20° on the tip-fin control surface had only a small effect on wing leeward patterns, and practically no influence of the deflection was detected on the tip-fin inboard surface at any angle of attack. Once again, oil flows for $\alpha = 30°$ are used as an illustration and are shown in figure 10. The primary separation line in figure 10(a) is drawn somewhat farther outboard near the wing trailing edge than for $\delta_{tf} = 0°$ in figure 3(a). This tends to force some of the wing-tip oil-flow patterns to slightly larger spanwise locations. However, this outward movement of surface patterns has a negligible impact on the inboard surface of the tip-fin, as indicated by a comparison of figures 10(b) and 3(b).

Oil flow on the tip-fin outboard surface for $\alpha = 20°$ and $\delta_{tf} = 20°$ is shown in figure 11. Flow reattachment just aft of the hinge line on the deflected surface of the tip-fin controller can be seen in figure 11(a). The reattachment line, from which flow radiates both forward and aft, extends to approximately one-half the tip-fin height. Streamwise flow from the leading edge of the unit prevails at higher locations. The control-surface deflection disrupts formation of the outboard reattachment line shown in figure 2(d) for $\alpha = 20°$ and $\delta_{tf} = 0°$. Flow separation also occurs on the tip-fin below the control surface. The associated separation line stops just short of the wing trailing edge, and a small reattachment pattern controls its aft portion. The three round spots aligned vertically on the tip-fin control surface (fig. 11(b)) mark the plaster-filled locations of screws holding the piece on the model. The oblique view in figure 11(b) shows that the separation below the tip-fin is caused by a division of flow at the lower edge of the deflected control surface. Also, flow reattachment occurs on the inboard interior surface of the tip-fin unit. Figure 11(c) shows the outboard portion of the tip-fin interior surface. It indicates a small region of attached flow along the lower edge of the deflected control element with separated flow filling the remainder of the region bounded by the inboard and outboard portions of the tip-fin structure. Similar interior flow patterns were found at all three angles of attack.

Outboard tip-fin oil-flow results for $\alpha = 30°$ and $\delta_{tf} = 20°$ are presented in figure 12. Separation occurs well ahead of the control-surface hinge line at upper locations on the tip-fin and moves aft to the hinge line at lower positions. Two lines of flow reattachment are visible on the deflected control surface, and both originate in the forward lower corner. One of the reattachment lines can be traced diagonally across the tip-fin to the upper aft corner of the control surface. The other reattachment line travels up the entire height of the tip-fin and is located a short distance aft of and parallel to the hinge line. The forward segment of the outboard flow reattachment noted at $\alpha = 30°$ and $\delta_{tf} = 0°$ in figure 3(c) has become established in figure 12 before reaching the lower forward corner of the deflected control surface. This may be related to the development of the diagonally oriented reattachment line across the tip-fin described previously and perhaps to the aft movement of primary flow separation over the tip-fin lower areas. Flow separation and reattachment are shown below the deflected control surface, similar to that for $\alpha = 20°$ in figure 11(a). However, the trailing end of the separation line in figure 12 has moved forward with the increase in angle of attack.

Figure 13 shows oil-flow patterns on the tip-fin outboard surface for $\alpha = 40°$ and $\delta_{tf} = 20°$. These surface flow directions resemble those in figure 12 for $\alpha = 30°$. Two reattachment lines are present on the control surface. One reattachment line runs diagonally to the aft upper corner of the tip-fin control surface, and the other branches off parallel to the control-surface hinge line. These two reattachment lines intersect a short distance above the lower edge of the control surface and very close to the hinge line. The diagonal reattachment line seems to be an extension of flow reattachment which develops near the tip-fin forward lower corner. Flow separation occurs ahead of the control surface only at locations above the point where the diagonal reattachment crosses the hinge line. The separation line below the control surface extends back only as far as the tip-fin structure, where it is abruptly cut off by attached flow from the wing windward surface.

Figure 14 presents thermographic-phosphor and thin-film-gauge heat-transfer test results corresponding to the oil-flow patterns in figure 13. The shaded areas, representing strips of locally higher heating identified by thermographic-phosphor, generally occur at the same locations as the oil-flow reattachment lines shown in figure 13. The thermographic-phosphor heating patterns lend support to the suggestion that the reattachment line which runs diagonally across the tip-fin control surface is an extension of flow reattachment initiated forward of the control-surface hinge line. However, there is no clear correlation of oil-flow patterns with the lowermost shaded strip in figure 14. The small circles show the locations of thin-film gauges on the tip-fin outboard surface. Normalized heating values, expressed as h/h_{ref}, are given for each location. The parameter h is the local heat-transfer coefficient and h_{ref} is the stagnation-point heat-transfer coefficient on a scaled 1-ft-radius sphere in the free stream. These data show that heating in areas associated with flow reattachment is typically two to four times higher than heating on other portions of the tip-fin outboard surface.

Oil-Flow Patterns for $\beta = 0°$, $\delta_e = 0°$, and $\delta_{tf} = 40°$

The effect of a tip-fin control-surface deflection equal to 40° on wing leeward and tip-fin inboard surface flow is virtually identical to that for $\delta_{tf} = 20°$. This can be seen by comparing the photographs in figure 15, using the oil flows for $\alpha = 30°$ for illustrative purposes, with the surface patterns in figure 10. Thus as before, the following discussion will concentrate on outboard tip-fin surface flow features.

Oil flows for $\alpha = 20°$ and $\delta_{tf} = 40°$ are shown in figure 16. The tip-fin geometry produces a very unusual double reattachment pattern that is evident in figure 16(a). Flow which separates near the tip-fin leading edge may be responsible for the curved reattachment line (concave forward) on the deflected control

surface where high reattachment heating rates may be expected. Surface flow from this reattachment is generally in an upward direction. The other reattachment pattern is located a short distance forward of the hinge line, and it wraps around the lower side of the tip-fin beneath the control surface. This pattern contains surface flow that is directed downward at all locations ahead of the hinge line, which is opposite to the control-surface reattachment. Another separation line forms slightly aft of the hinge line where the opposing flows of these two reattachments meet. However, a portion of the reversed flow from the control-surface reattachment spills over onto the tip-fin at locations ahead of the hinge line near the top of the unit where it turns upward and leaves the tip-fin. Immediately below is downward flow associated with the forward reattachment. It is uncertain if a stagnation point forms at the intersection of the upward- and downward-traveling flows ahead of the hinge line, or if flow from the control-surface reattachment turns sharply to merge with both patterns. The oblique view in figure 16(b) indicates a greater extent of flow reattachment on the tip-fin interior surface for $\delta_{tf} = 40°$ than for the 20° deflection shown in figure 11(b). Downward flow from the interior-surface reattachment pattern separates along a common boundary with reattaching flow located below the deflected surface.

Flow patterns at $\alpha = 30°$ and $\delta_{tf} = 40°$ are shown in figure 17. The outboard reattachment has changed considerably from that shown in figure 16 because of the increase in angle of attack. Flow reattachment on the deflected control surface is quite prominent. It appears that the upward-moving and reversed surface flow generated by the reattachment extends forward to the line of flow separation aft of the tip-fin leading edge, though there was very little oil movement in this low-shear area. Establishment of the forward portion of the "zero-deflection" flow reattachment pattern over the tip-fin forward lower corner moves the boundary of separated flow in this region back to the control-surface hinge line. There is no indication that the zero-deflection reattachment pattern extends beyond the hinge line. That portion of the lower-corner zero-deflection reattachment flow that is turned downward forms a secondary vortex reattachment below the deflected surface as a result of interaction with upward-moving flow from the wing windward flow field.

Oil-flow photographs for $\alpha = 40°$ and $\delta_{tf} = 40°$ are illustrated in figure 18. The single reattachment pattern has moved forward on the control surface at this angle of attack. The onset of the zero-deflection reattachment is located higher on the tip-fin forward lower corner at $\alpha = 40°$, and it seems to force the primary flow-separation line farther aft than at lower angles of attack. A secondary vortex reattachment similar to that for $\alpha = 30°$ occurs below the deflected control surface. As for $\alpha = 40°$ and $\delta_{tf} = 20°$, the secondary flow pattern is interrupted by attached flow from the wing windward surface upon reaching the tip-fin trailing edge. The tip-fin interior surfaces at $\alpha = 40°$ and $\delta_{tf} = 40°$ are shown in figures 18(b) and 18(c). The reattachment pattern in figure 18(b) covers nearly the entire inboard portion of the interior surface area. A comparison of figure 18(b) with figure 16(b) illustrates how increasing angle of attack results in more extensive flow coverage of the tip-fin interior surface. Figure 18(c) depicts a similar situation on the outboard interior surface, but with attached flow from the deflected control-surface lower edge. This situation tends to increase heating rates to the tip-fin interior surfaces.

Concluding Remarks

This report contains an analysis of oil-flow patterns obtained on a proposed tip-fin controller for the Space Shuttle orbiter. These tests were conducted at Mach 10 in air for a free-stream Reynolds number of 1.13×10^6 at 20°, 30°, and 40° angle of attack and sideslip angles of 0° and 2°. The effect of elevon deflections at −10°, 0°, and 10° and of tip-fin control-surface deflections of 0°, 20°, and 40° on surface flow directions were investigated. A comparison of tip-fin heating data obtained at $\alpha = 40°$ and $\delta_{tf} = 20°$ with the corresponding oil-flow patterns was also performed.

It was established that the tip-fin has very little effect on wing leeward flow patterns. Sideslip angles up to 2° produce some asymmetries in wing leeward patterns, tip-fin inboard surface flow separation, and outward flow reattachment locations, but none of the observed effects should result in a significant change in heating compared with the case for $\beta = 0°$. Elevon deflections of −10°, 0°, and 10° had no influence on tip-fin surface flow patterns. The highest heating rates on the tip-fin outboard surface are expected to result from strong flow interactions caused by control-surface deflections. Prominent reattachment lines were observed in oil flow on the tip-fin deflected control surface for $\delta_{tf} = 20°$ and 40°. These patterns displayed a close correspondence with thermographic-phosphor and thin-film-gauge results at test conditions of $\alpha = 40°$ and $\delta_{tf} = 20°$. Heating levels in the reattachment zones appeared to be roughly two to four times higher than those in areas not associated with flow reattachment. The lower edge of the deflected control surface was also subjected to an adverse thermal environment as was the tip-fin leading edge. Increasing the tip-fin control-surface deflection angle and increasing angle of attack exposes the interior surfaces of the unit to a greater degree of secondary

flow patterns generated by the outer-surface interactions. Some consideration of thermal protection in this area may be required as well.

Langley Research Center
National Aeronautics and Space Administration
Hampton, VA 23665
September 26, 1984

References

1. Powell, Richard W.; and Freeman, Delma C., Jr.: Application of a Tip-Fin Controller to the Shuttle Orbiter for Improved Yaw Control. AIAA-81-0074, Jan. 1981.

2. Powell, Richard W.; and Freeman, Delma C., Jr.: Evaluation of the Aerodynamic Control of the Space Shuttle Orbiter With Tip-Fin Controllers. AIAA-84-0488, Jan. 1984.

3. Freeman, Delma C., Jr.; and Powell, Richard W.: Impact of Far-Aft Center of Gravity for a Single-Stage-To-Orbit Vehicle. *J. Spacecr. & Rockets*, vol. 17, no. 4, July–Aug. 1980, pp. 311–315.

4. Whittliff, Charles E.: Heat Transfer Measurements on a Tip-Fin-Controller for the Space Shuttle Orbiter. AIAA-84-1752, June 1984.

5. Schaefer, William T.: *Characteristics of Major Active Wind Tunnels at the Langley Research Center.* NASA TM X-1130, 1965.

6. Dunavant, James C.; and Stone, Howard W.: *Effect of Roughness on Heat Transfer to Hemisphere Cylinders at Mach Numbers 10.4 and 11.4.* NASA TN D-3871, 1967.

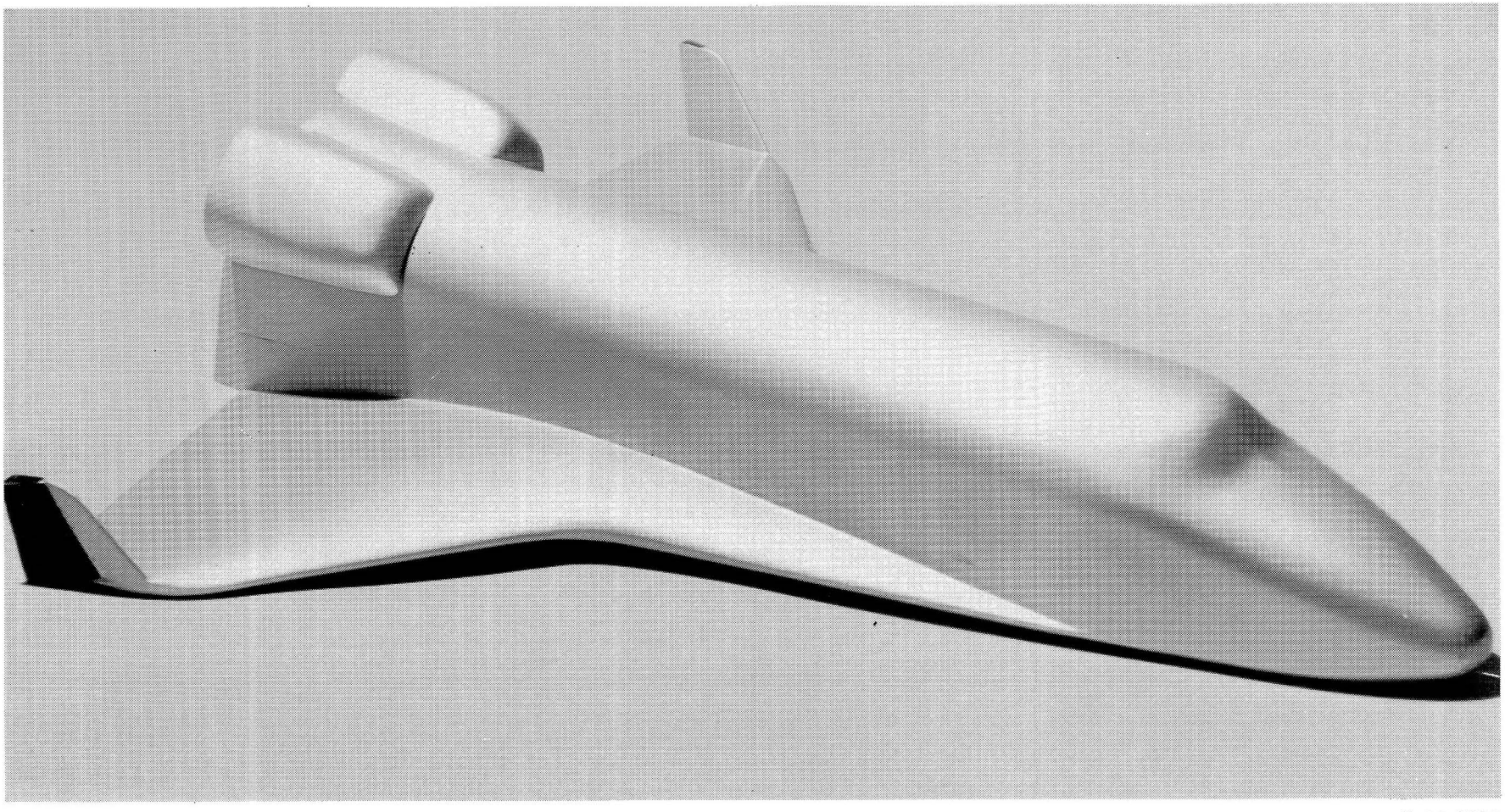

L-80-6580

(a) Model with tip-fins installed.

Figure 1. Space Shuttle orbiter model and tip-fins.

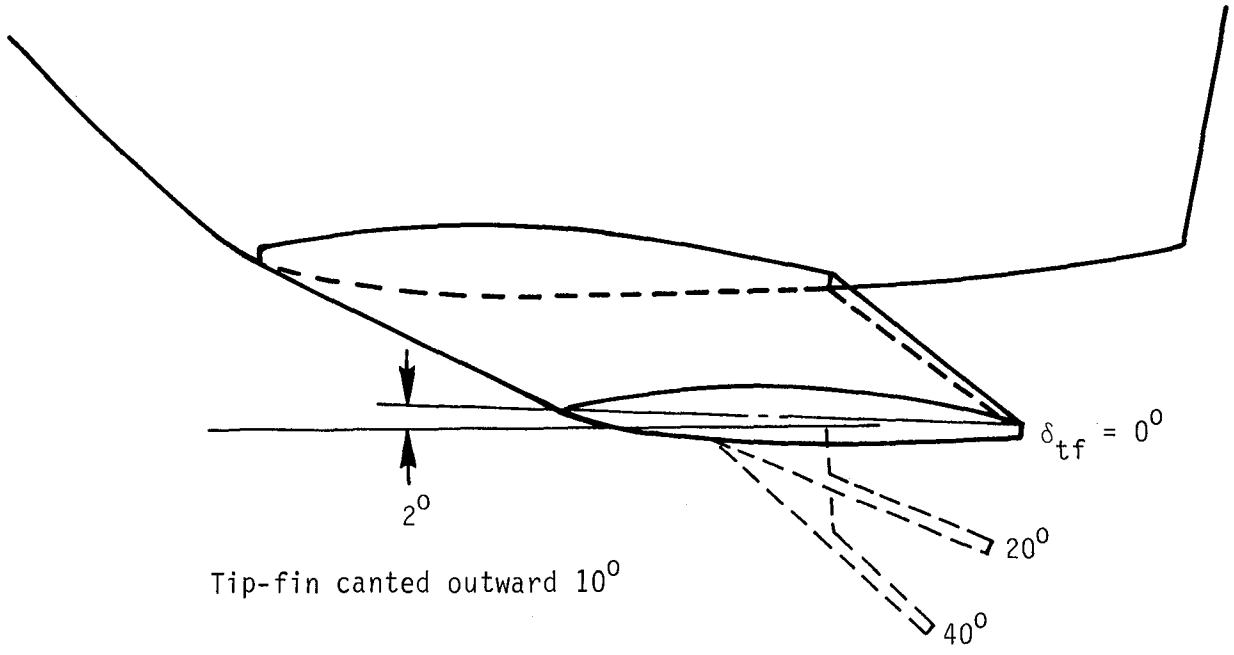

(b) Top view of tip-fin showing control-surface deflection angles.

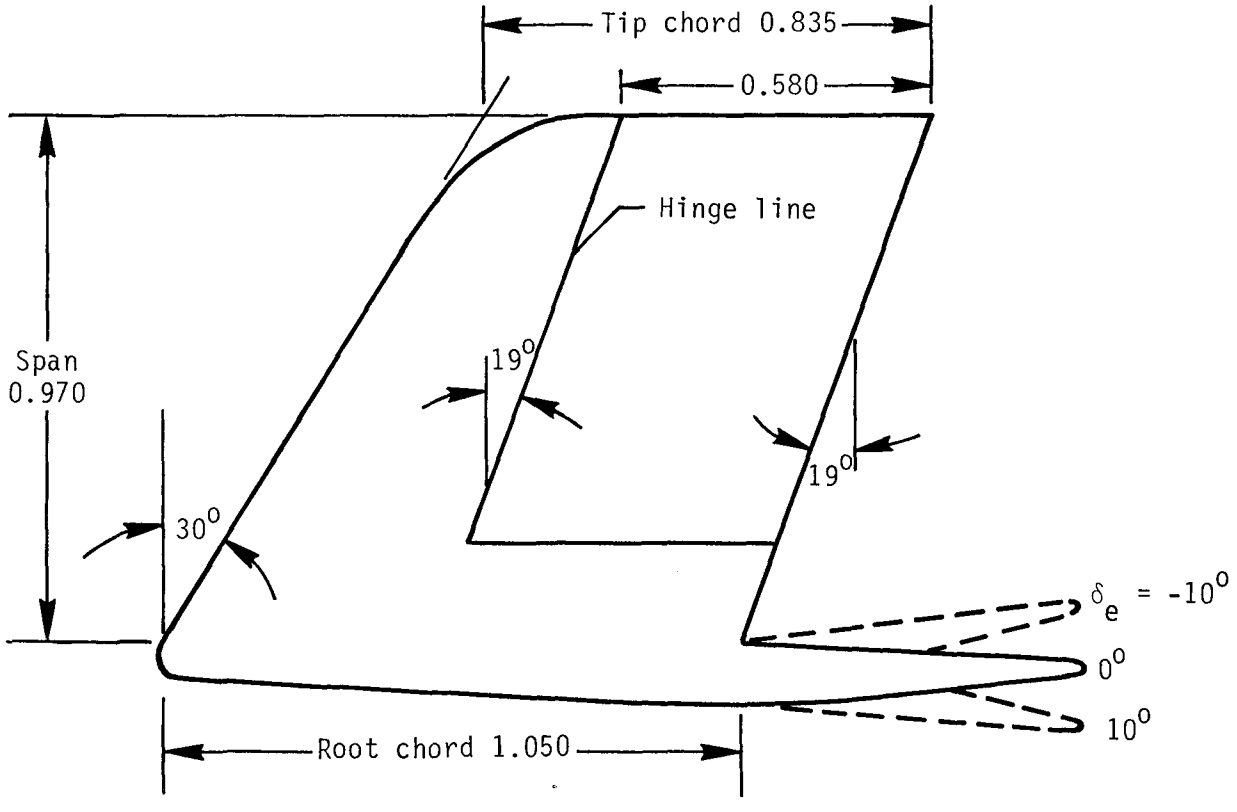

(c) Side view of tip-fin showing elevon deflection angles. Linear dimensions are in inches.

Figure 1. Concluded.

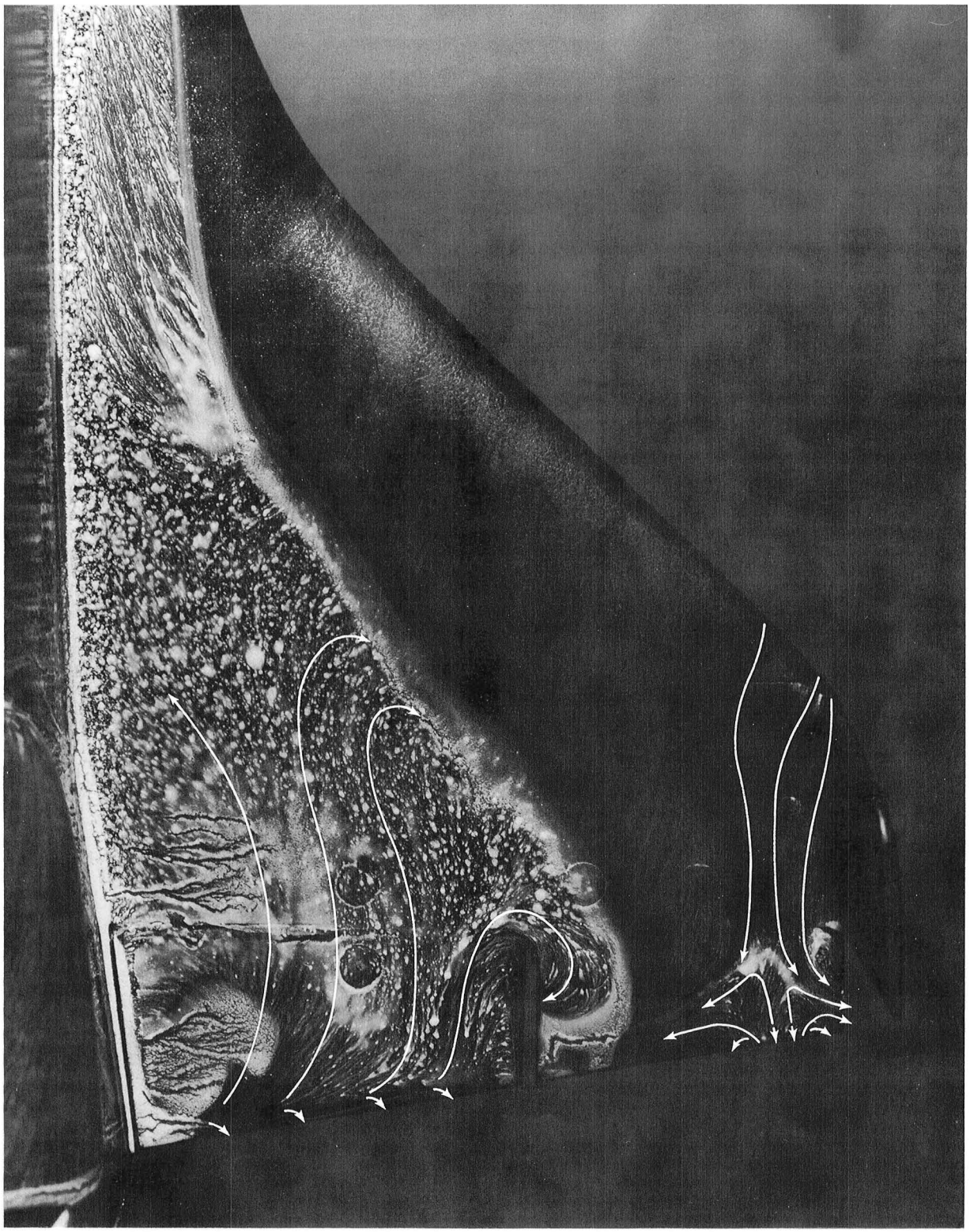

L-84-136

(a) Wing leeward surface.

Figure 2. Oil-flow patterns at $\alpha = 20°$ for $\beta = 0°$, $\delta_e = 0°$, and $\delta_{tf} = 0°$.

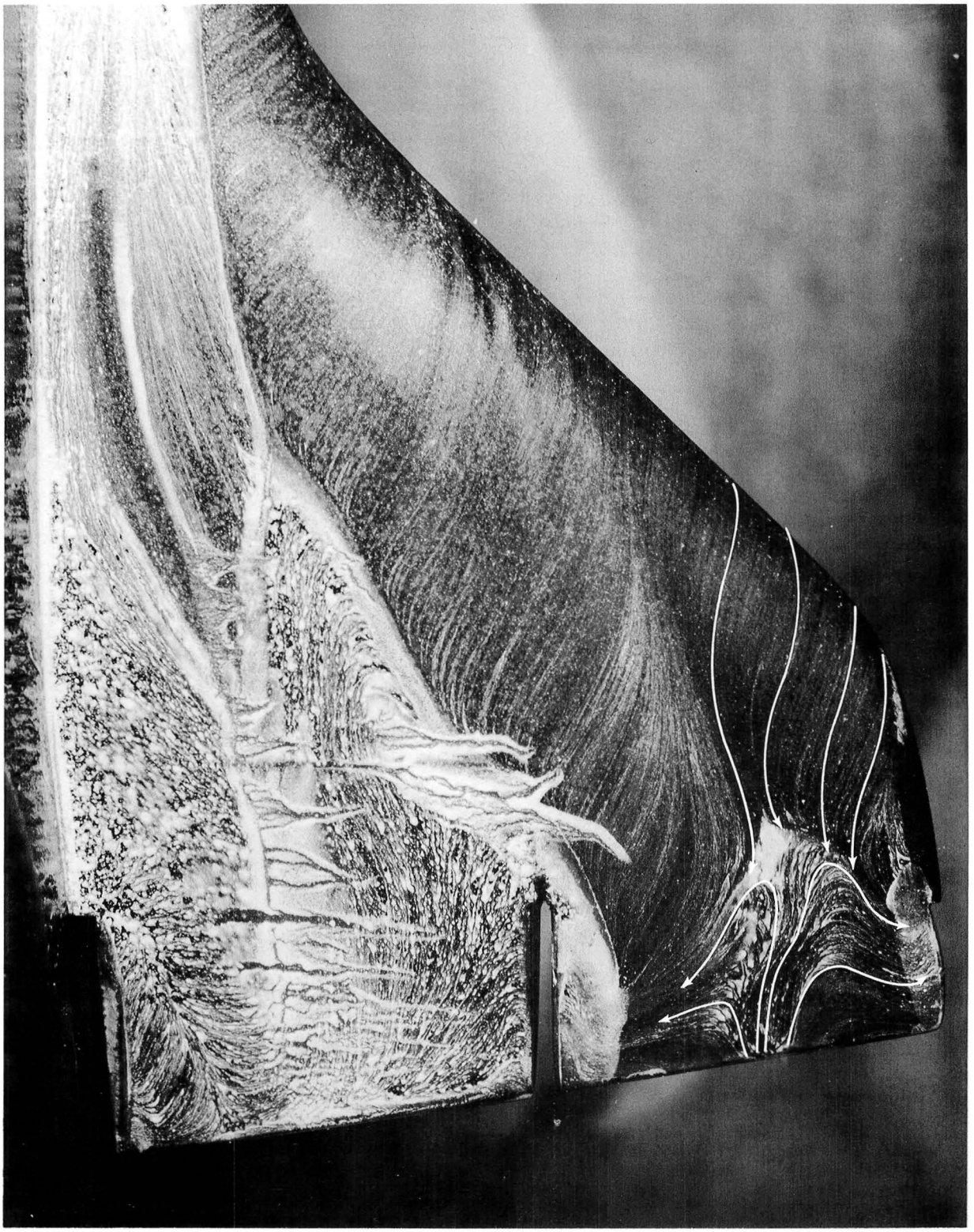

L-84-137

(b) Wing leeward surface with no tip-fin at $\alpha = 20°$ and $Re_\infty = 2.37 \times 10^6$.

Figure 2. Continued.

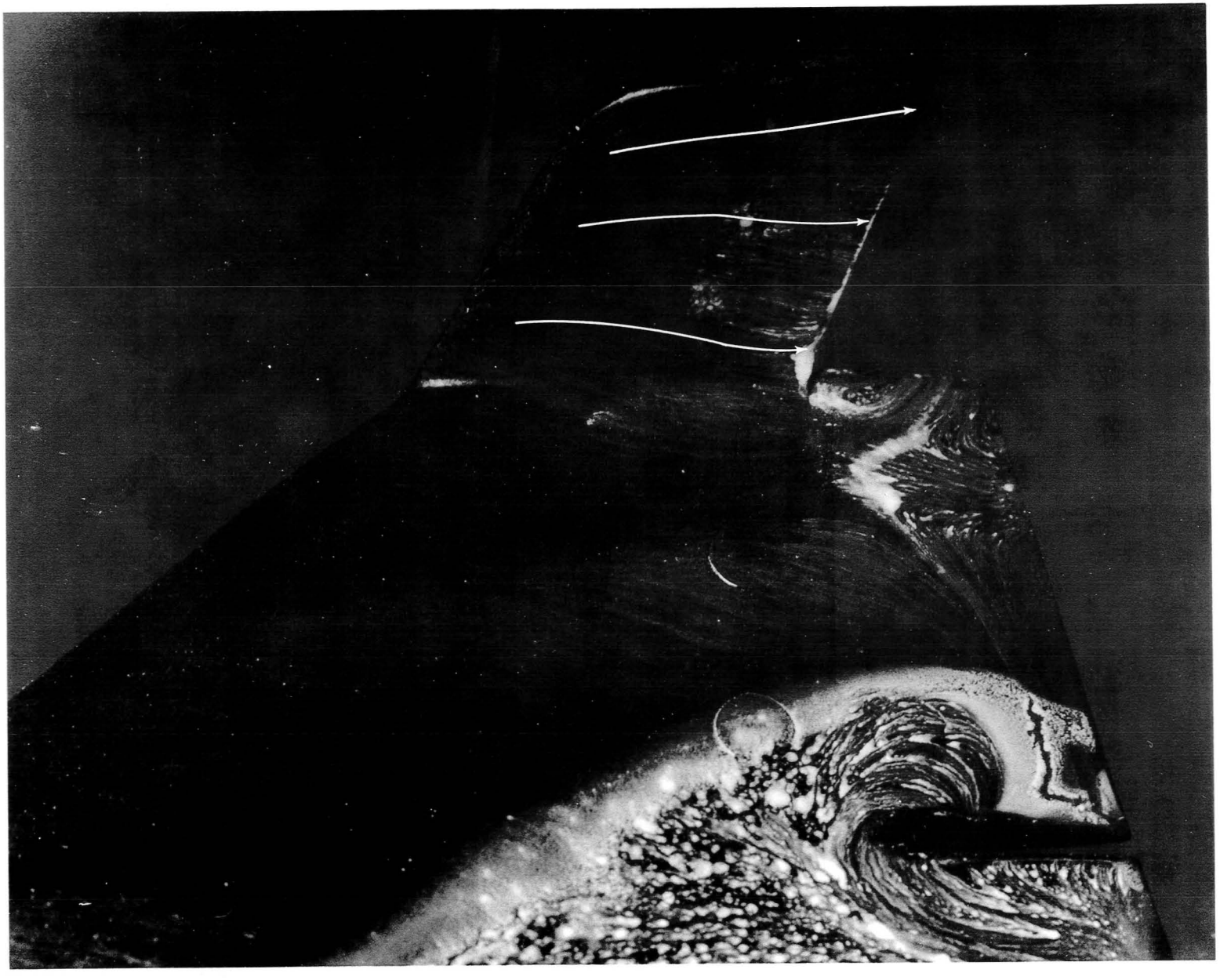

L-84-138

(c) Tip-fin inboard surface.

Figure 2. Continued.

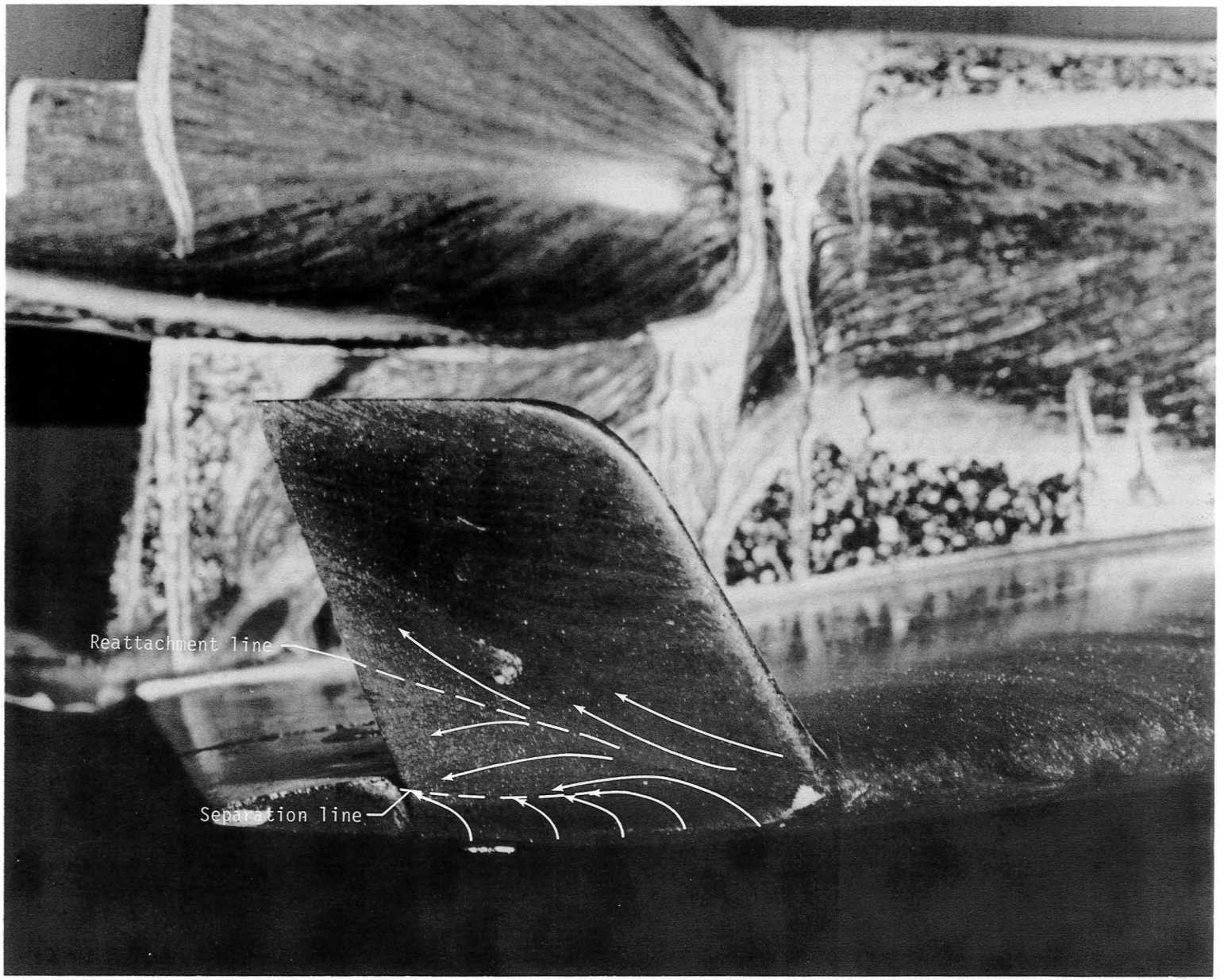

L-84-139

(d) Tip-fin outboard surface.

Figure 2. Concluded.

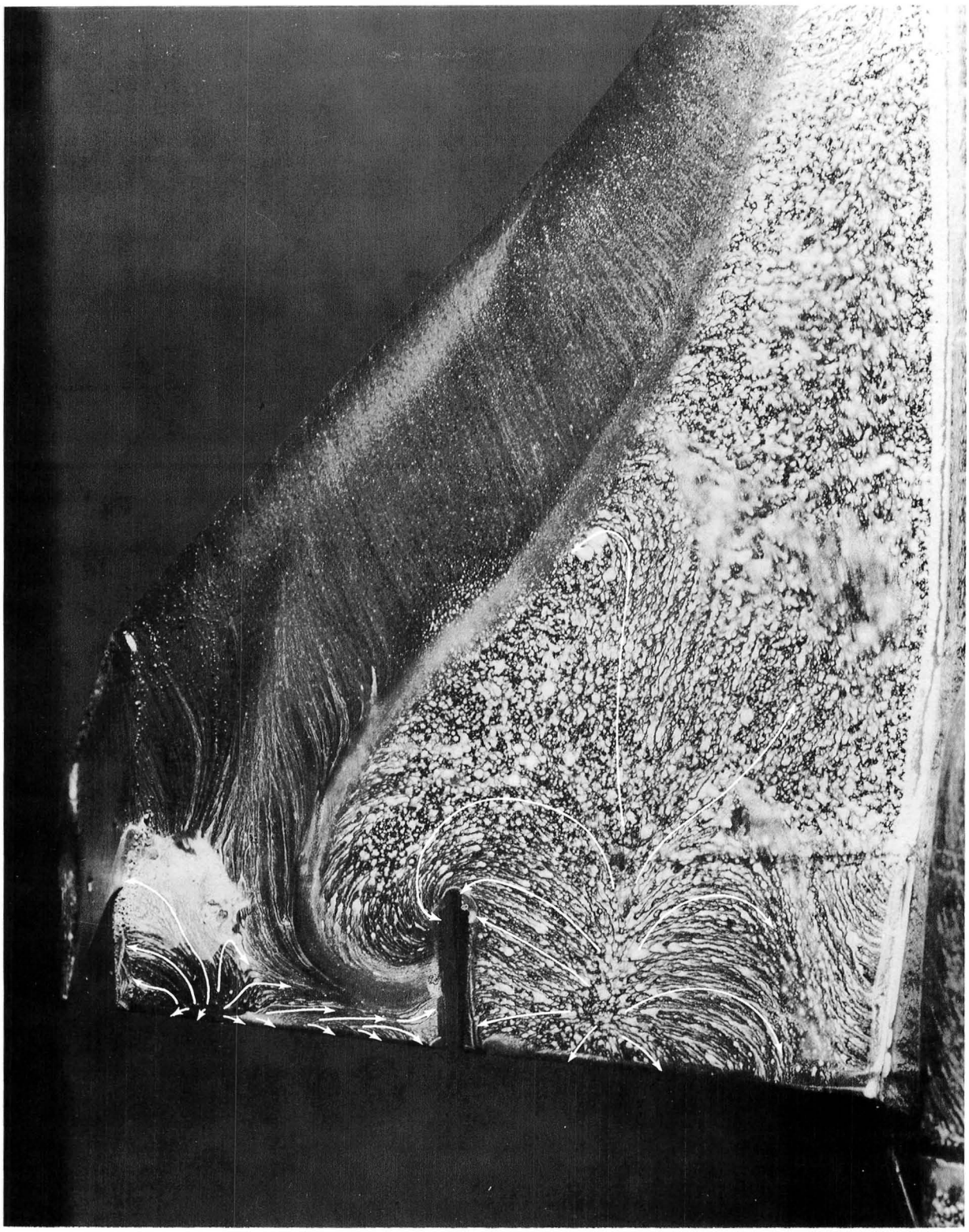

L-84-140

(a) Wing leeward surface.

Figure 3. Oil-flow patterns at $\alpha = 30°$ for $\beta = 0°$, $\delta_e = 0°$, and $\delta_{tf} = 0°$.

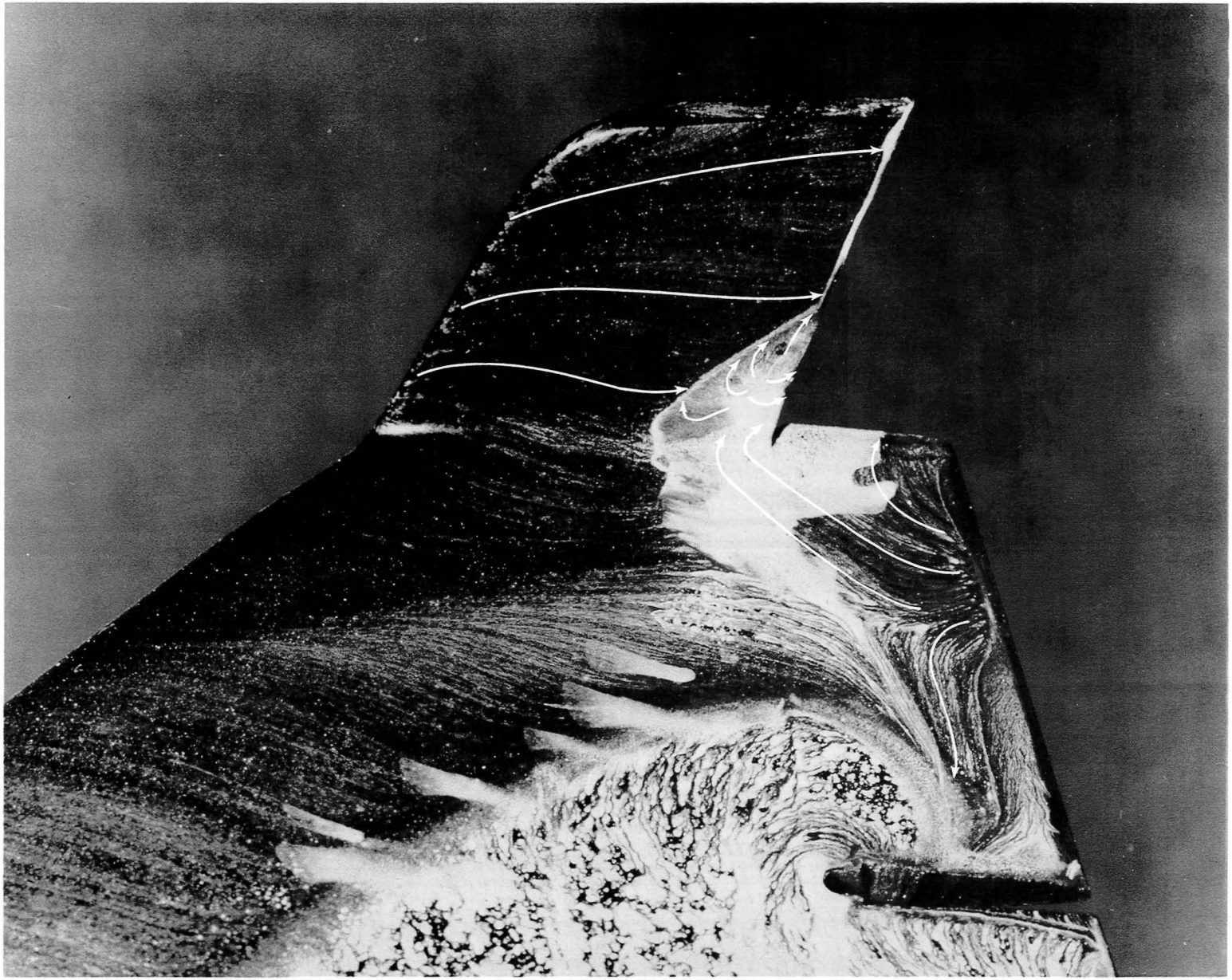

L-84-141

(b) Tip-fin inboard surface.

Figure 3. Continued.

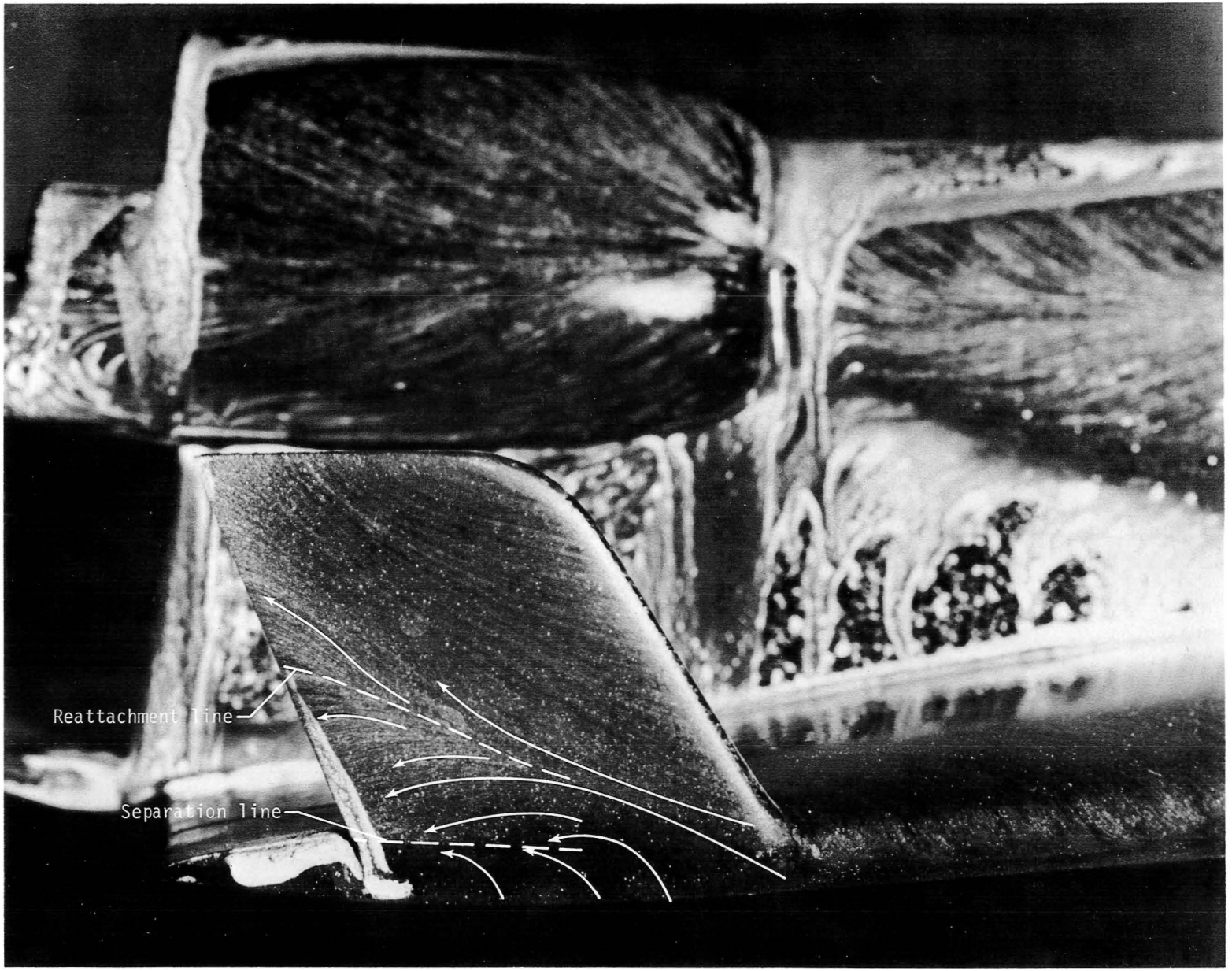

L-84-142

(c) Tip-fin outboard surface.

Figure 3. Concluded.

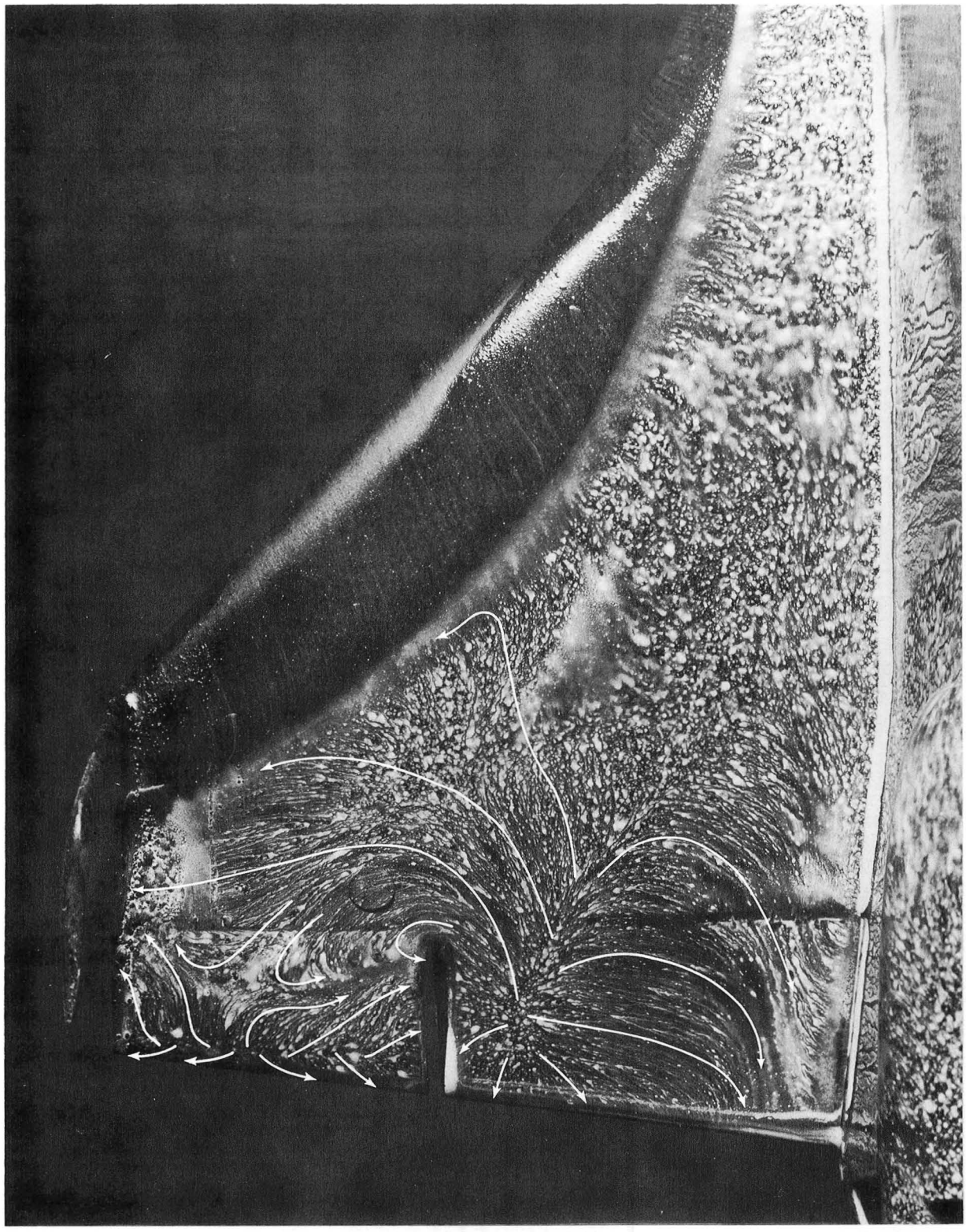

L-84-143

(a) Wing leeward surface.

Figure 4. Oil-flow patterns at $\alpha = 40°$ for $\beta = 0°$, $\delta_e = 0°$, and $\delta_{tf} = 0°$.

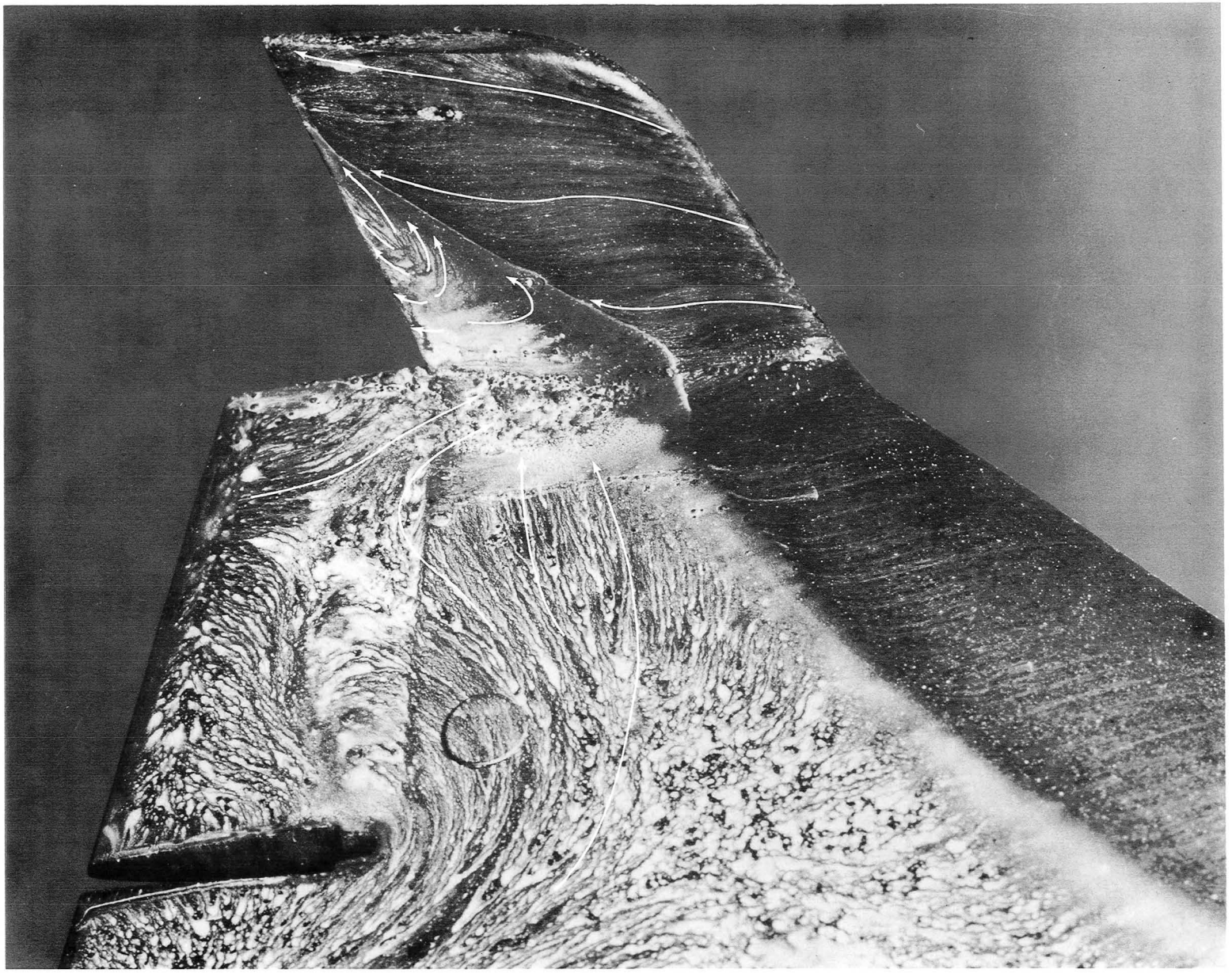

L-84-144

(b) Tip-fin inboard surface.

Figure 4. Continued.

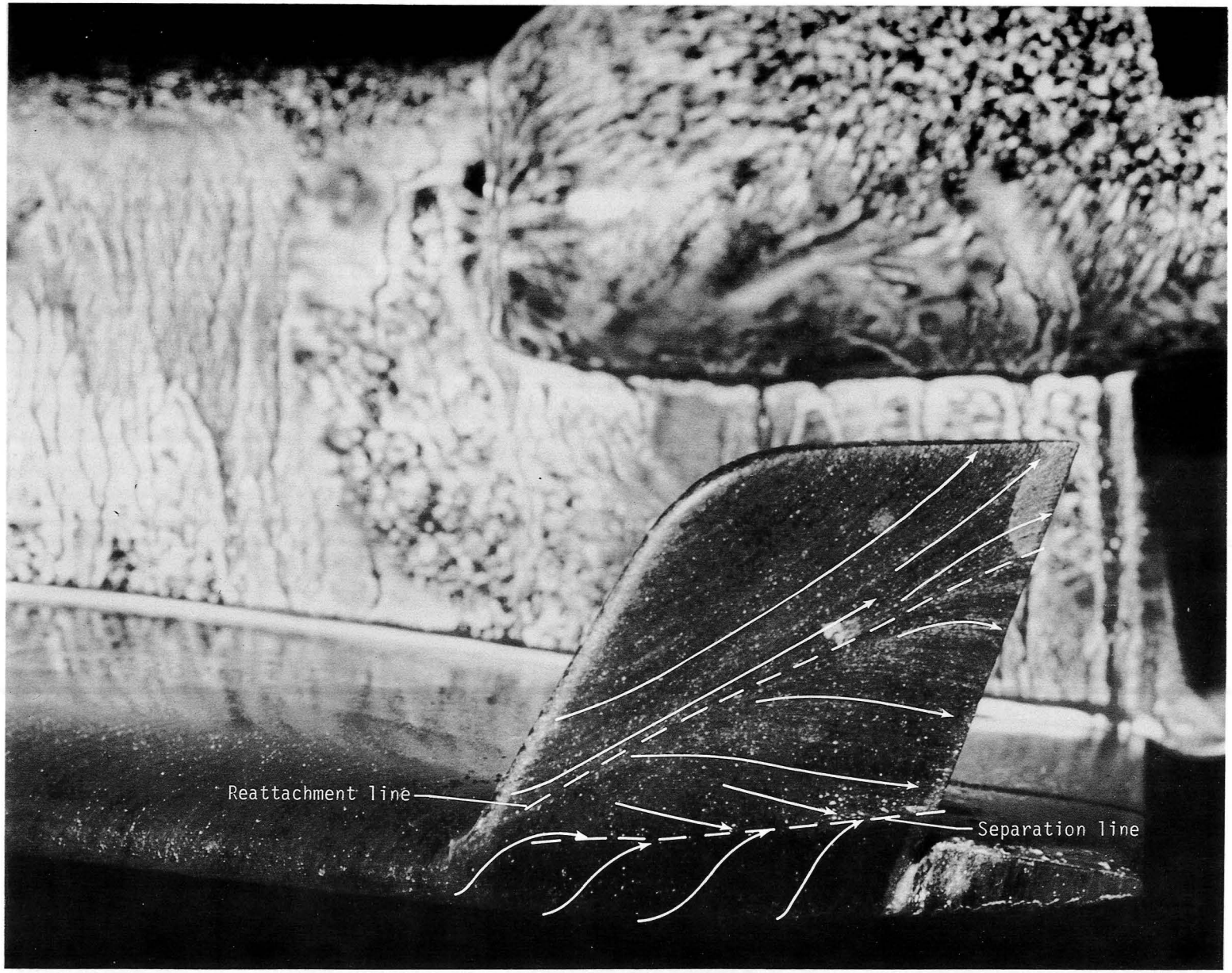

L-84-145

(c) Tip-fin outboard surface.

Figure 4. Concluded.

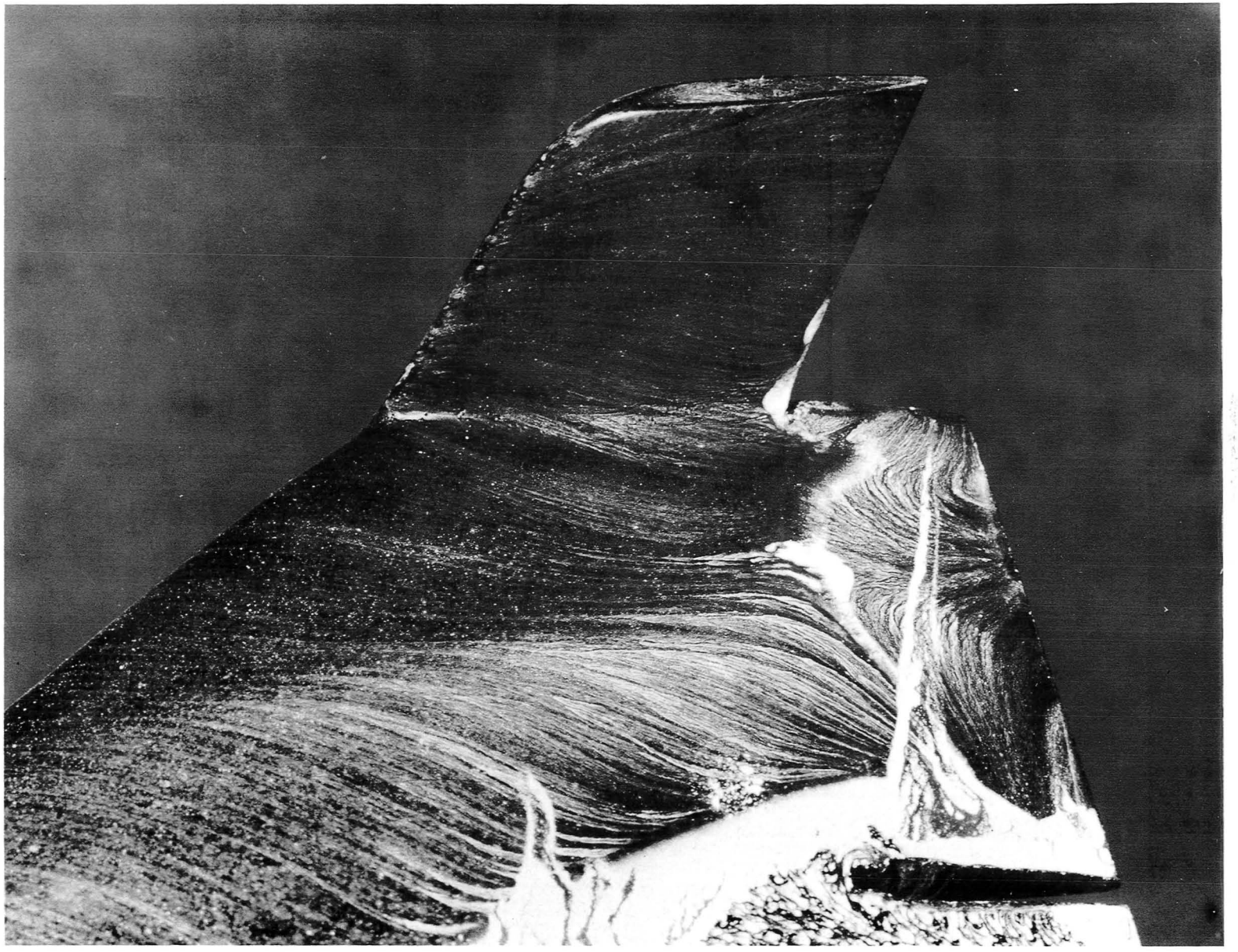

L-84-146

(a) Inboard surface of right tip-fin.

Figure 5. Oil-flow patterns at $\alpha = 20°$ for $\beta = 2°$, $\delta_e = 0°$, and $\delta_{tf} = 0°$.

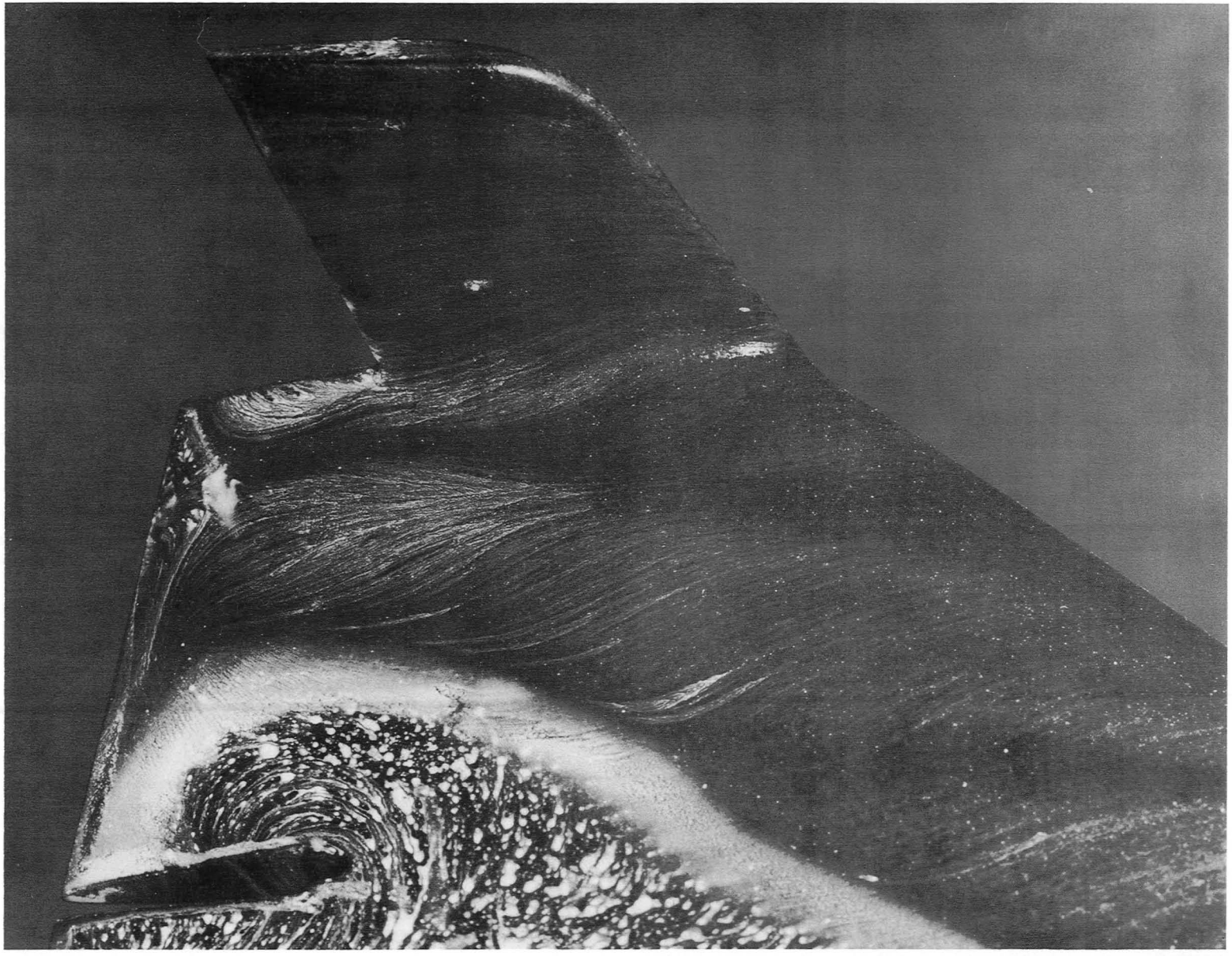

L-84-147

(b) Inboard surface of left tip-fin.

Figure 5. Continued.

L-84-148

(c) Outboard surface of right tip-fin.

Figure 5. Continued.

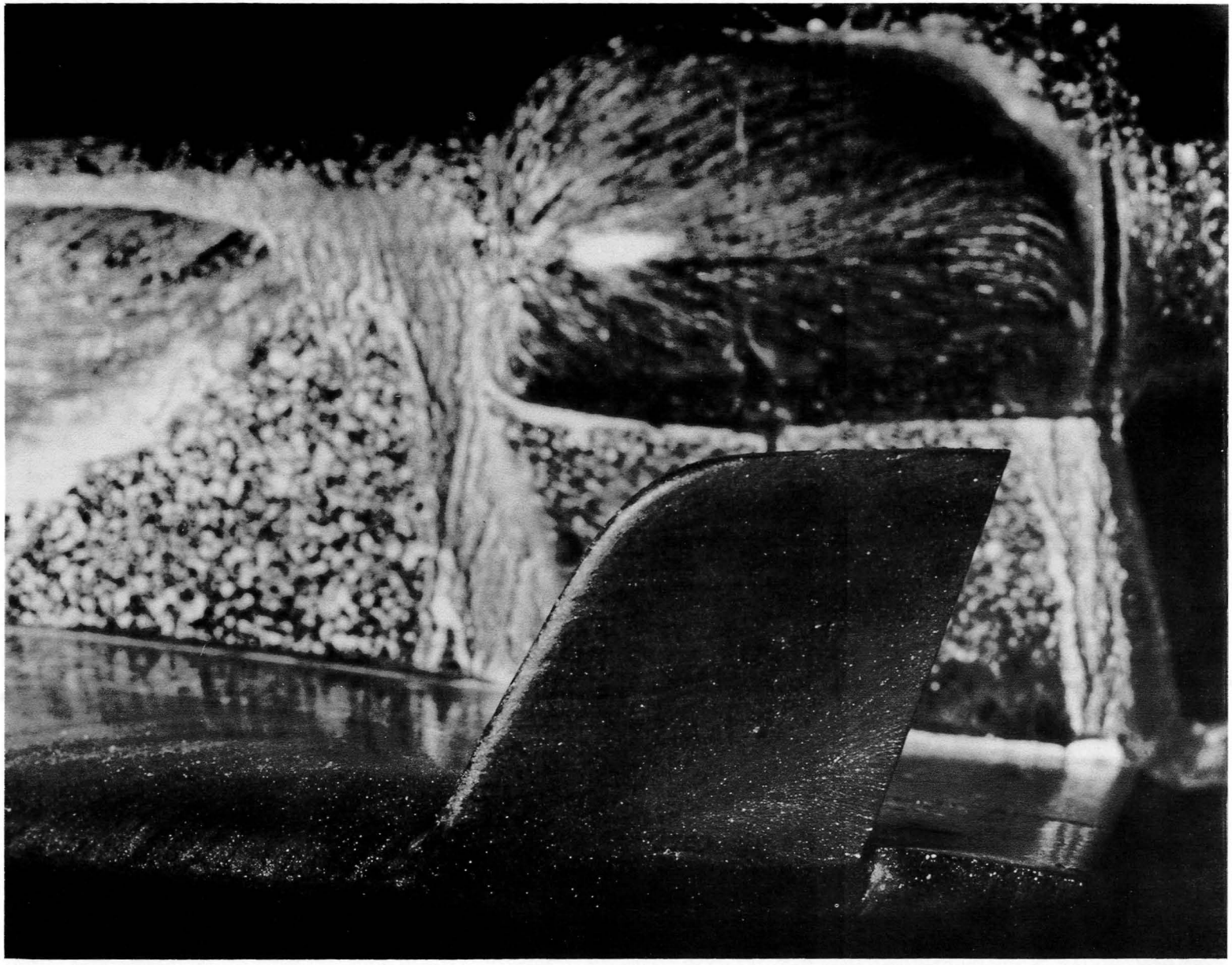

L-84-149

(d) Outboard surface of left tip-fin.

Figure 5. Concluded.

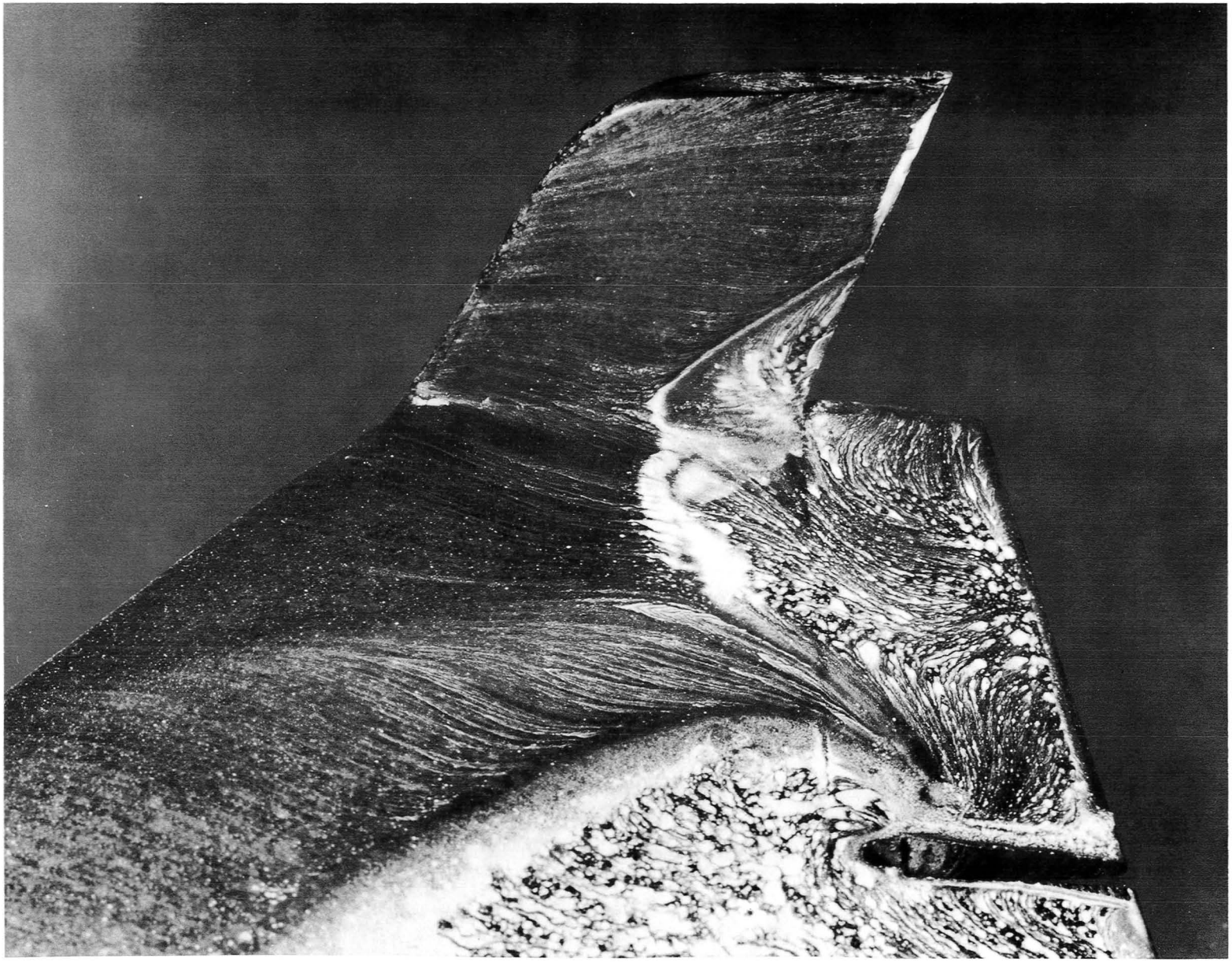

L-84-10,601

(a) Inboard surface of right tip-fin.

Figure 6. Oil-flow patterns at $\alpha = 30°$ for $\beta = 2°$, $\delta_e = 0°$, and $\delta_{tf} = 0°$.

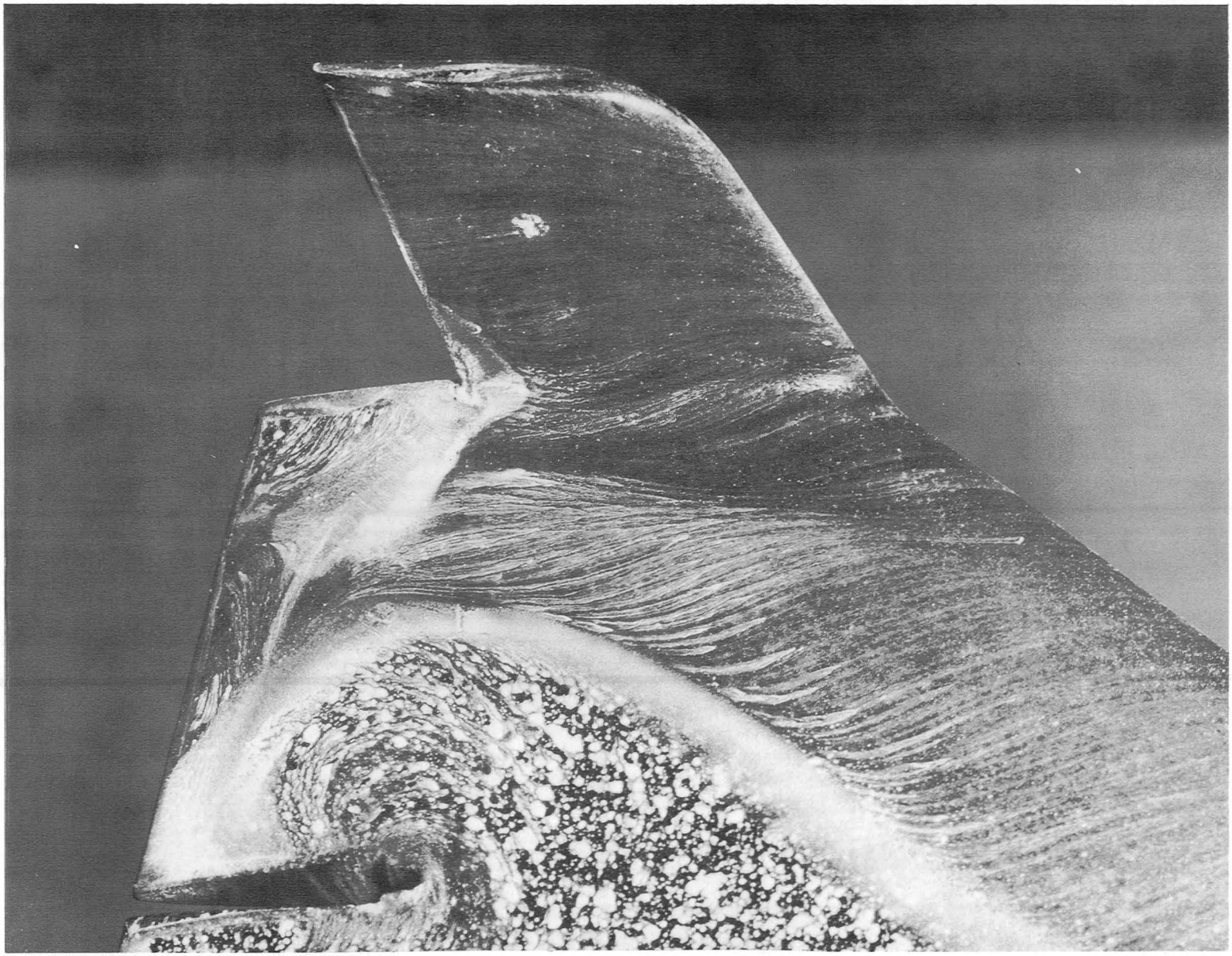

L-84-10,602

(b) Inboard surface of left tip-fin.

Figure 6. Continued.

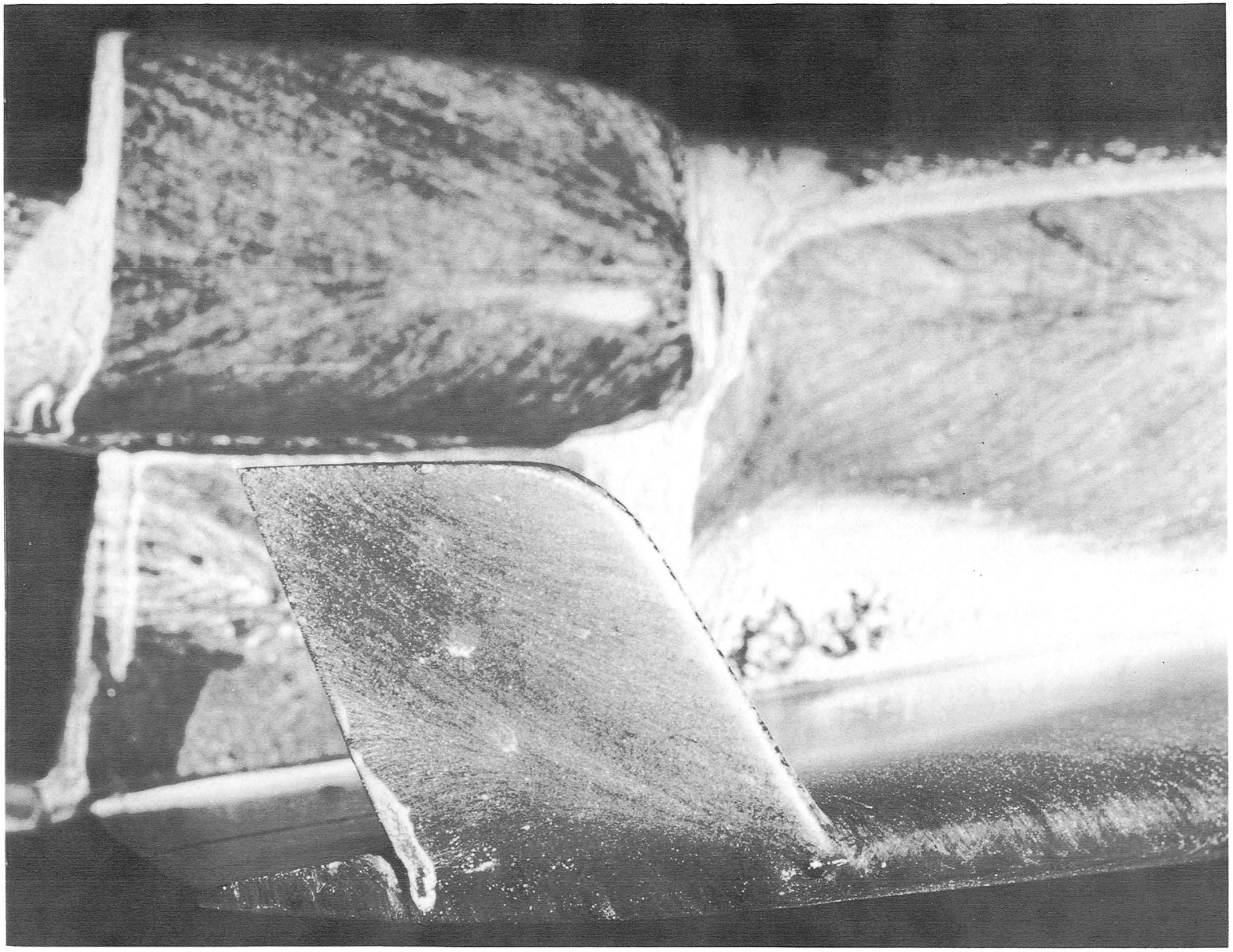

L-84-10,603

(c) Outboard surface of right tip-fin.

Figure 6. Continued.

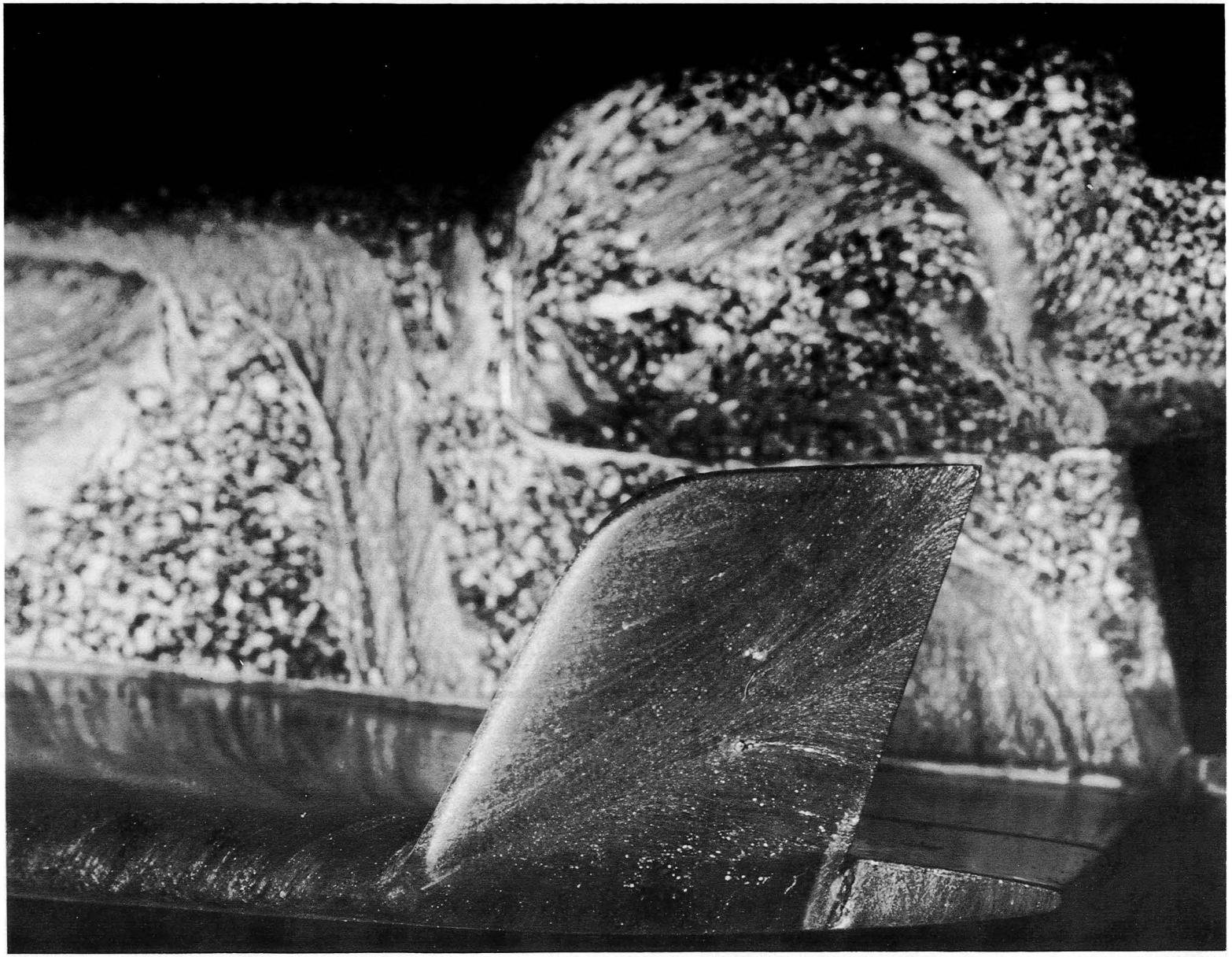

L-84-10,604

(d) Outboard surface of left tip-fin.

Figure 6. Concluded.

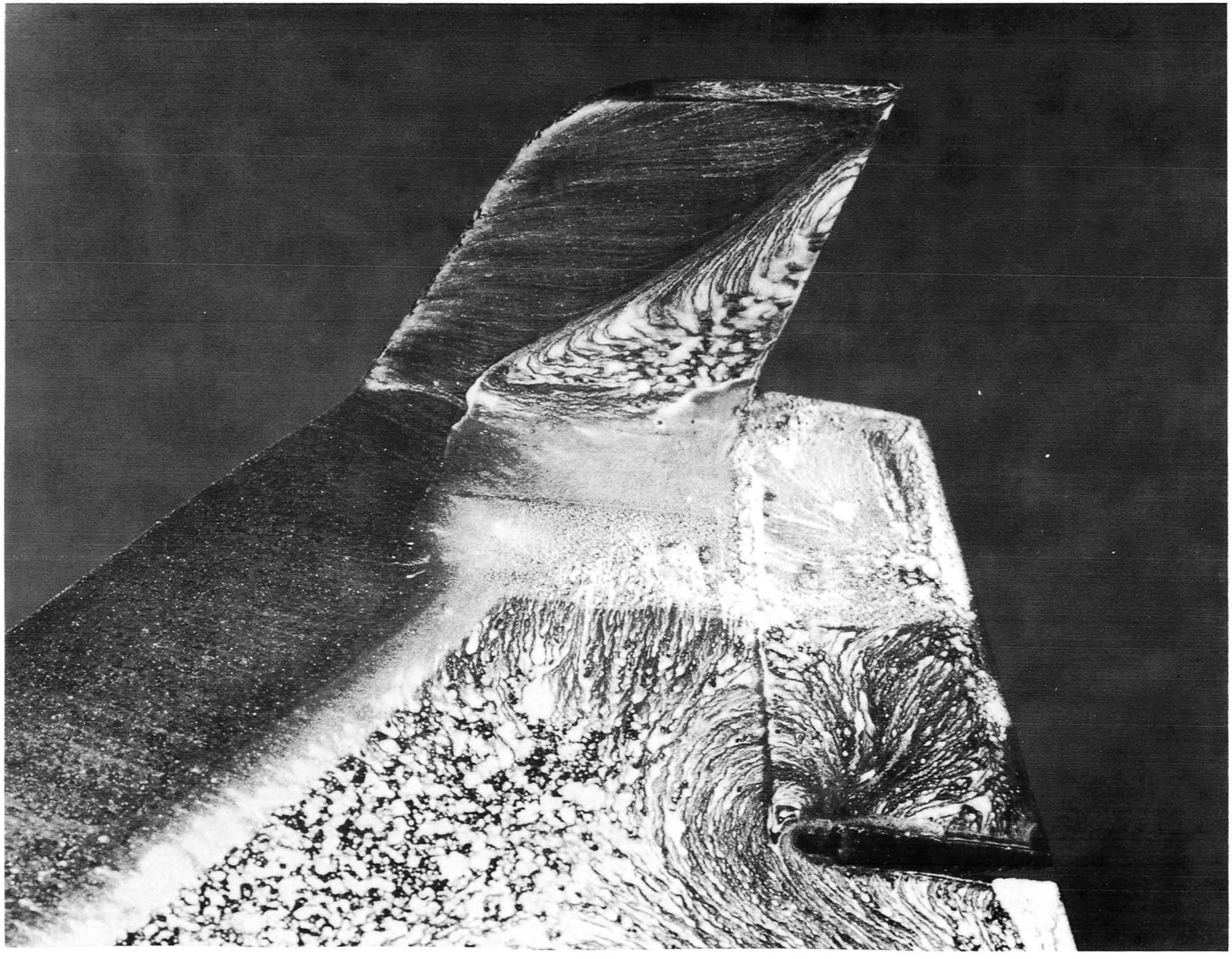

L-84-10,605

(a) Inboard surface of right tip-fin.

Figure 7. Oil-flow patterns at $\alpha = 40°$ for $\beta = 2°$, $\delta_e = 0°$, and $\delta_{tf} = 0°$.

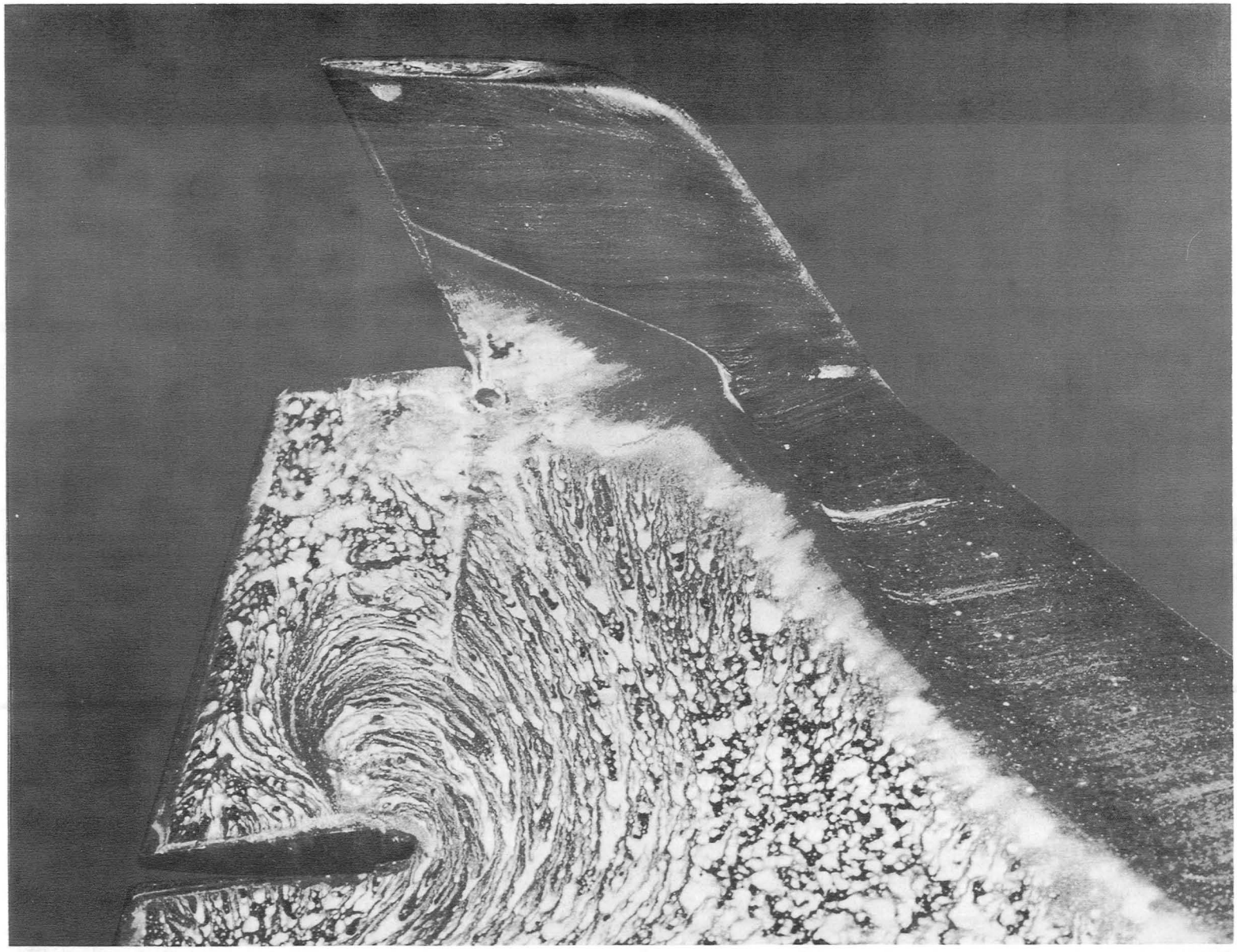

L-84-10,606

(b) Inboard surface of left tip-fin.

Figure 7. Continued.

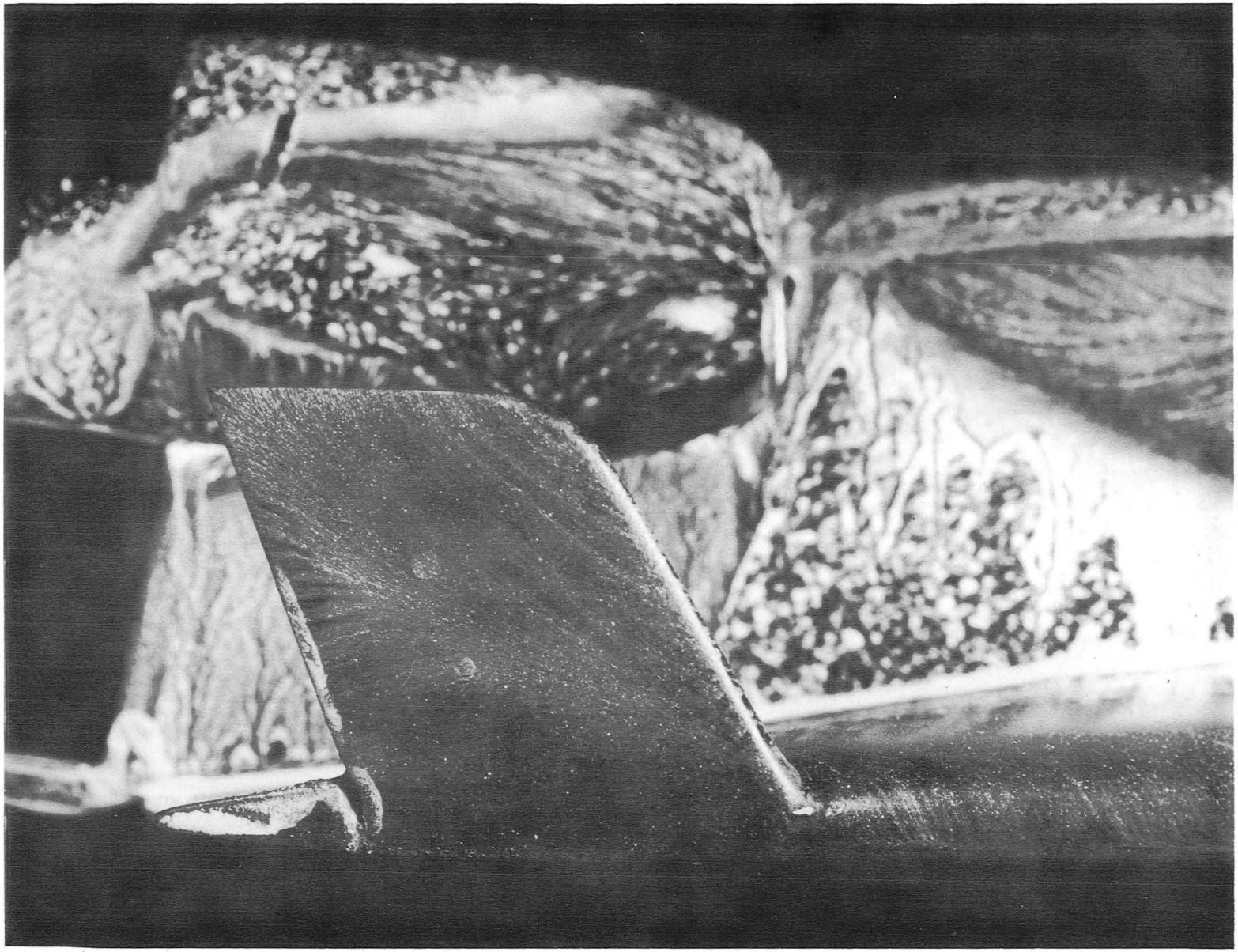

L-84-10,607

(c) Outboard surface of right tip-fin.

Figure 7. Continued.

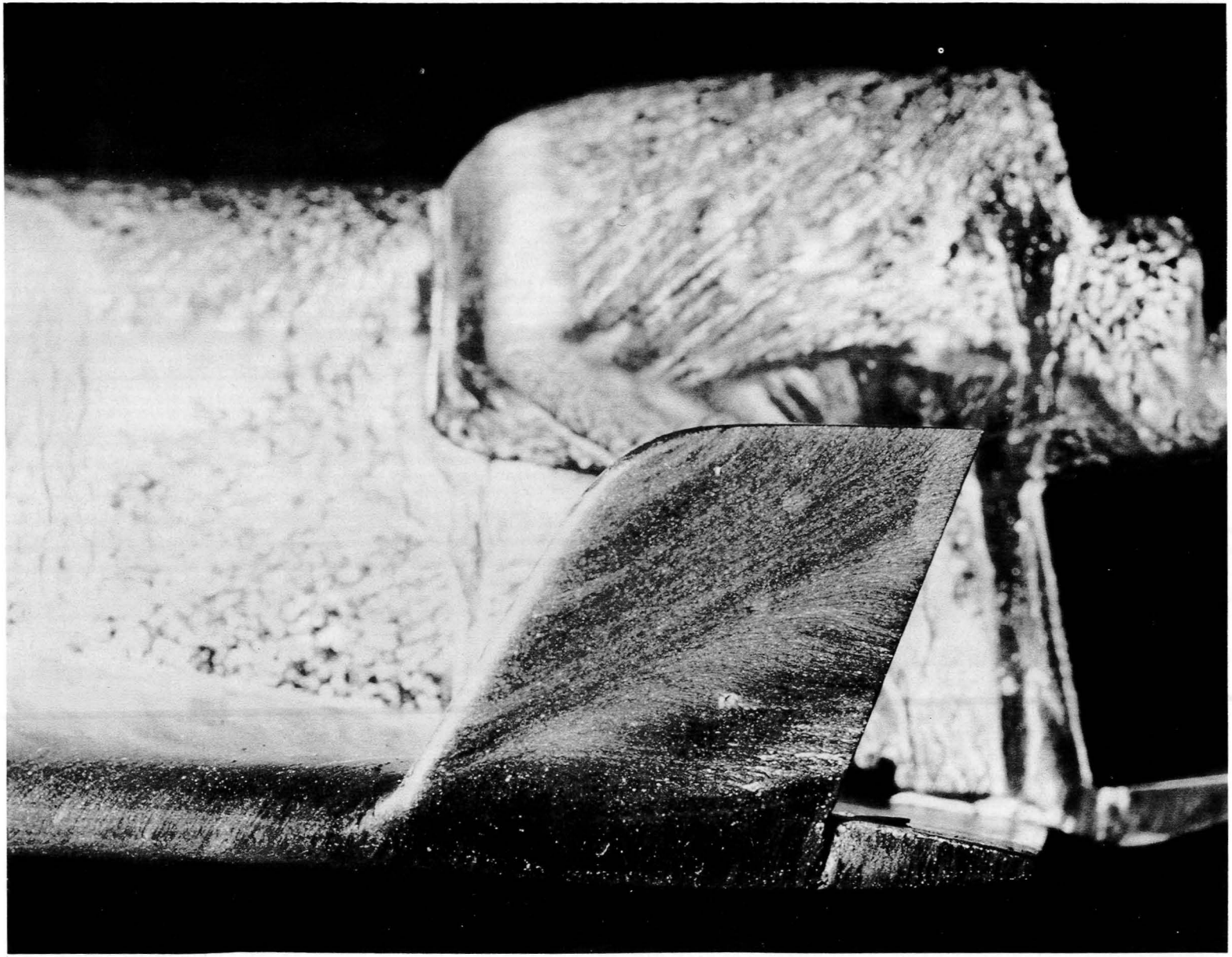

L-84-10,608

(d) Outboard surface of left tip-fin.

Figure 7. Concluded.

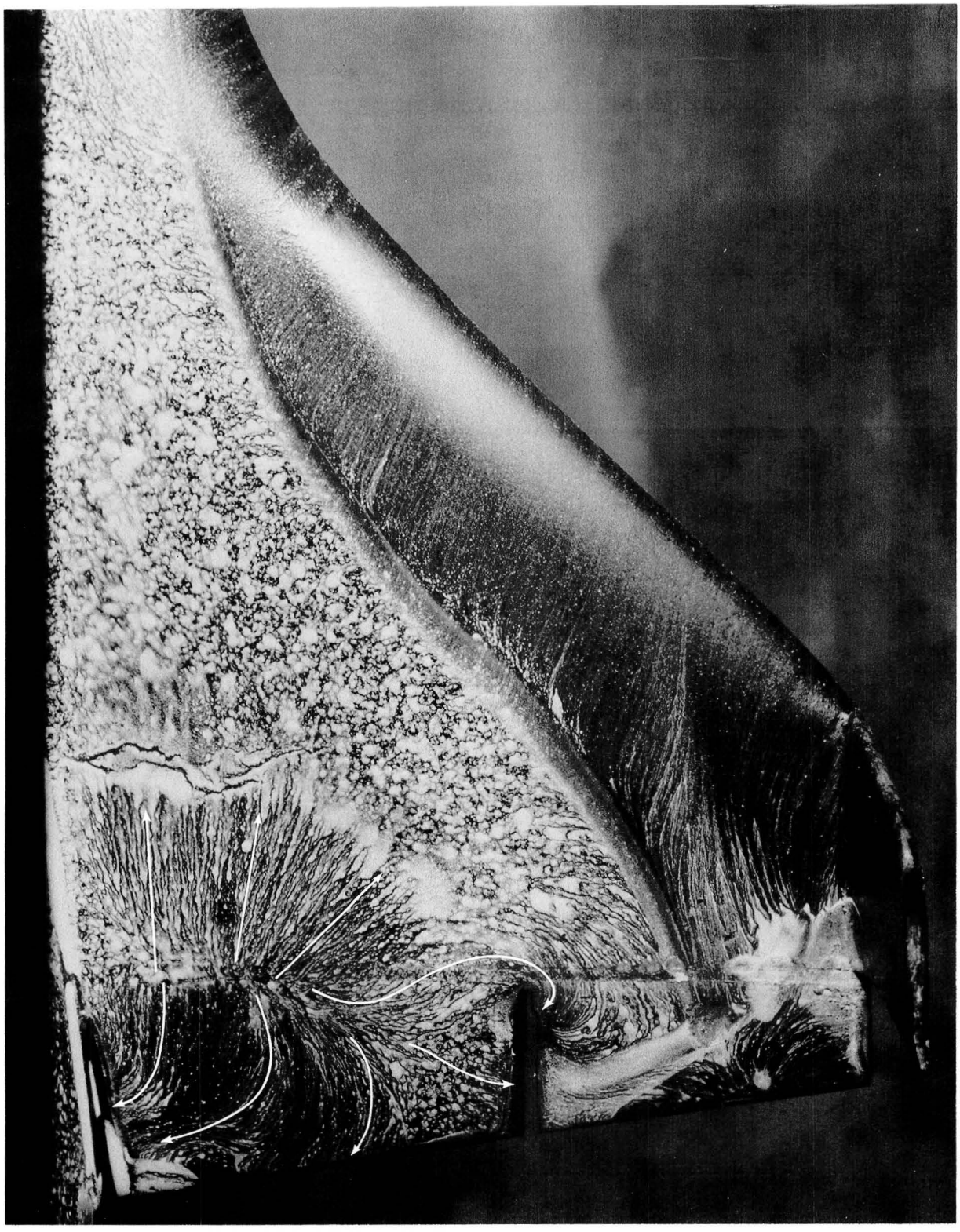

L-84-10,609

(a) Wing leeward surface.

Figure 8. Oil-flow patterns at $\alpha = 30°$ for $\beta = 0°$, $\delta_e = 10°$, and $\delta_{tf} = 0°$.

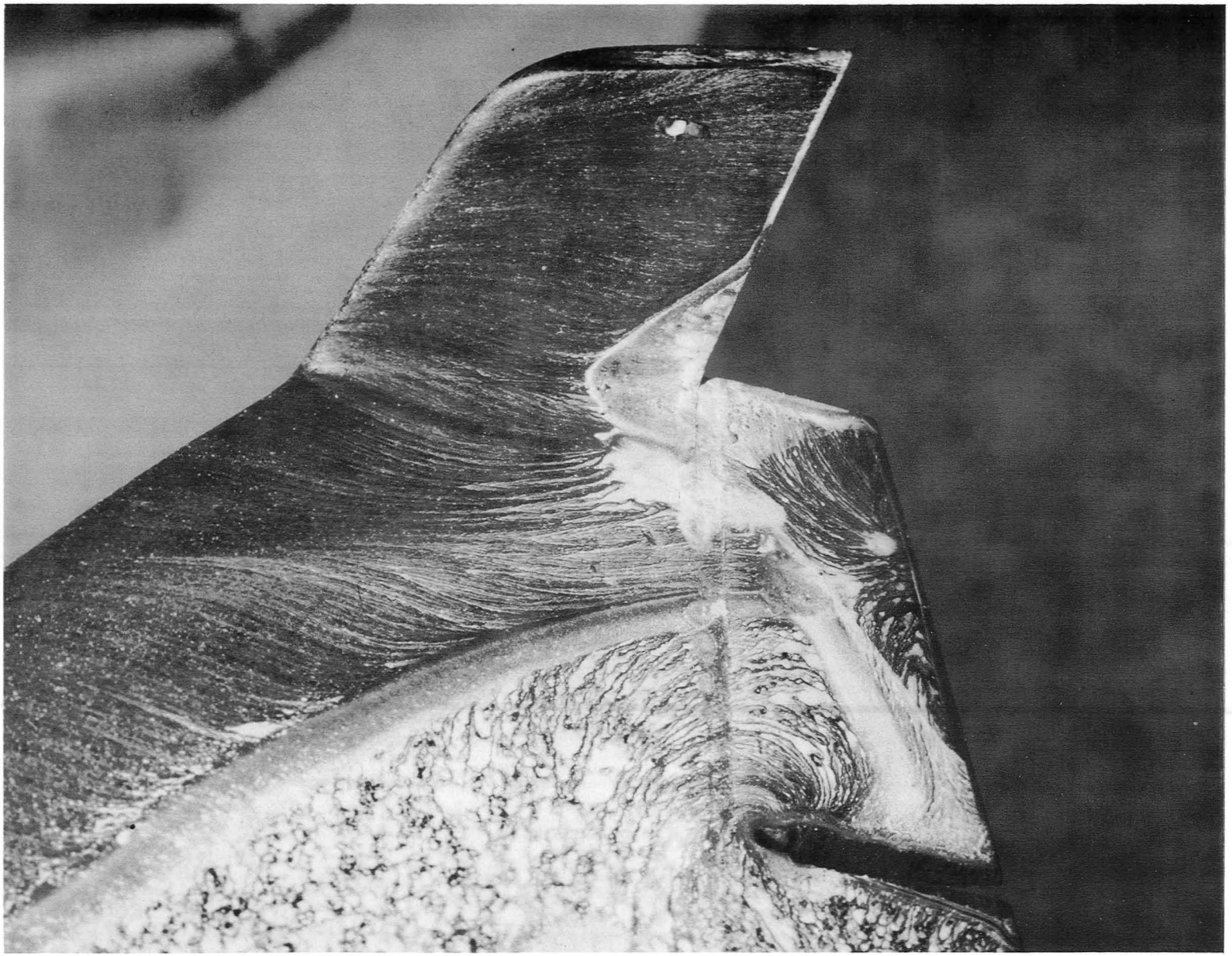

L-84-10,610

(b) Tip-fin inboard surface.

Figure 8. Continued.

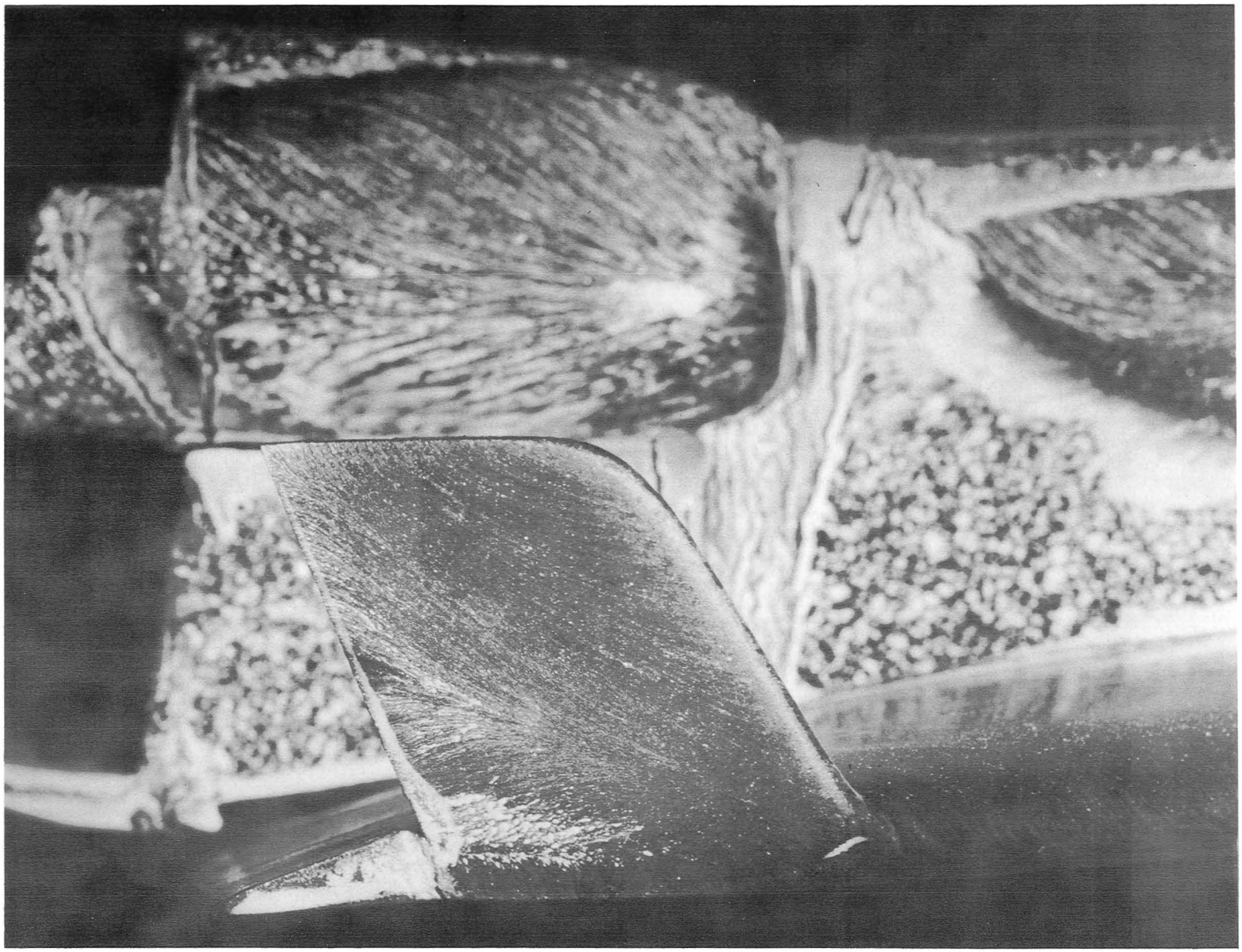

L-84-10,611

(c) Tip-fin outboard surface.

Figure 8. Concluded.

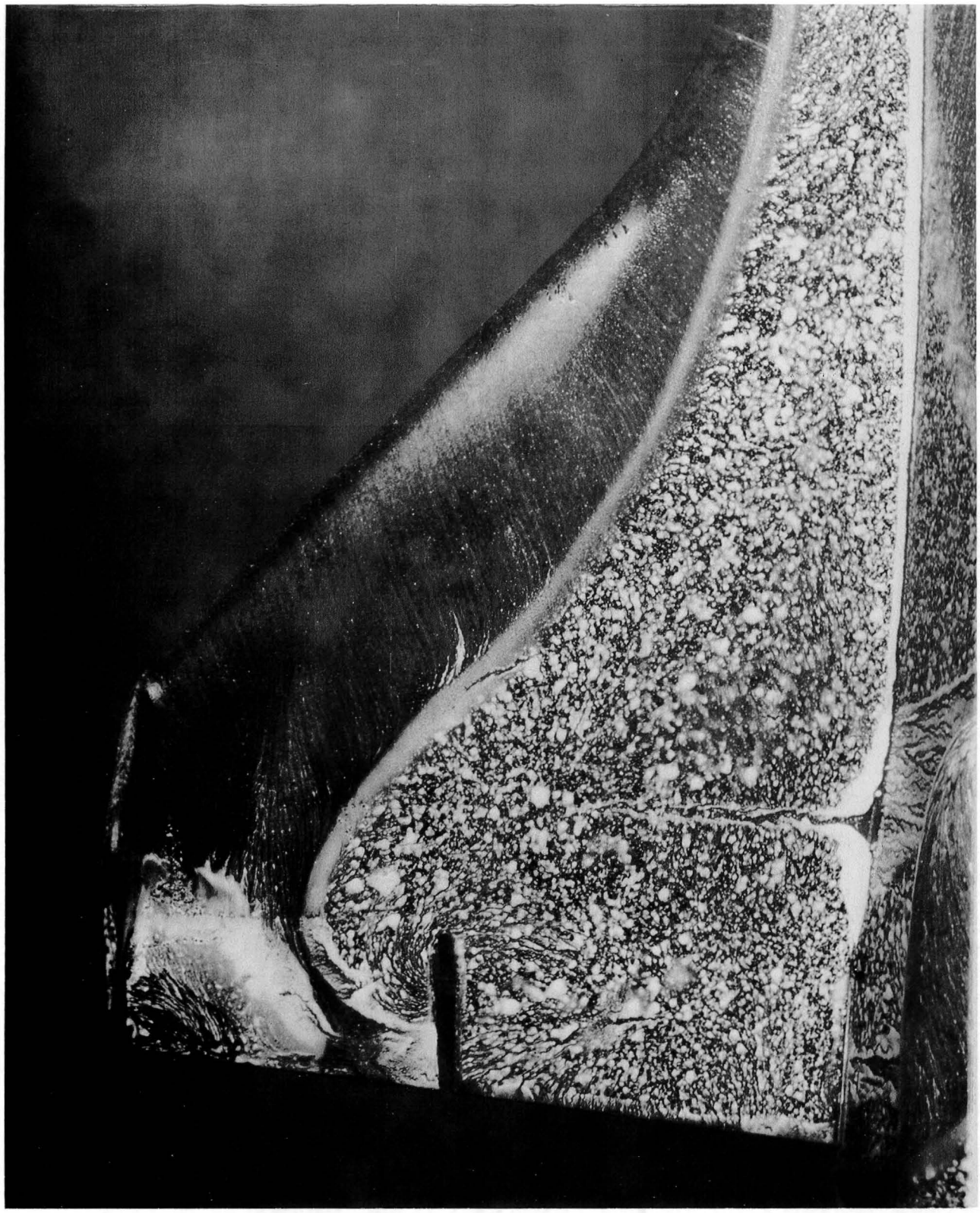

L-84-10,612

(a) Wing leeward surface.

Figure 9. Oil-flow patterns at $\alpha = 30°$ for $\beta = 0°$, $\delta_e = -10°$, and $\delta_{tf} = 0°$.

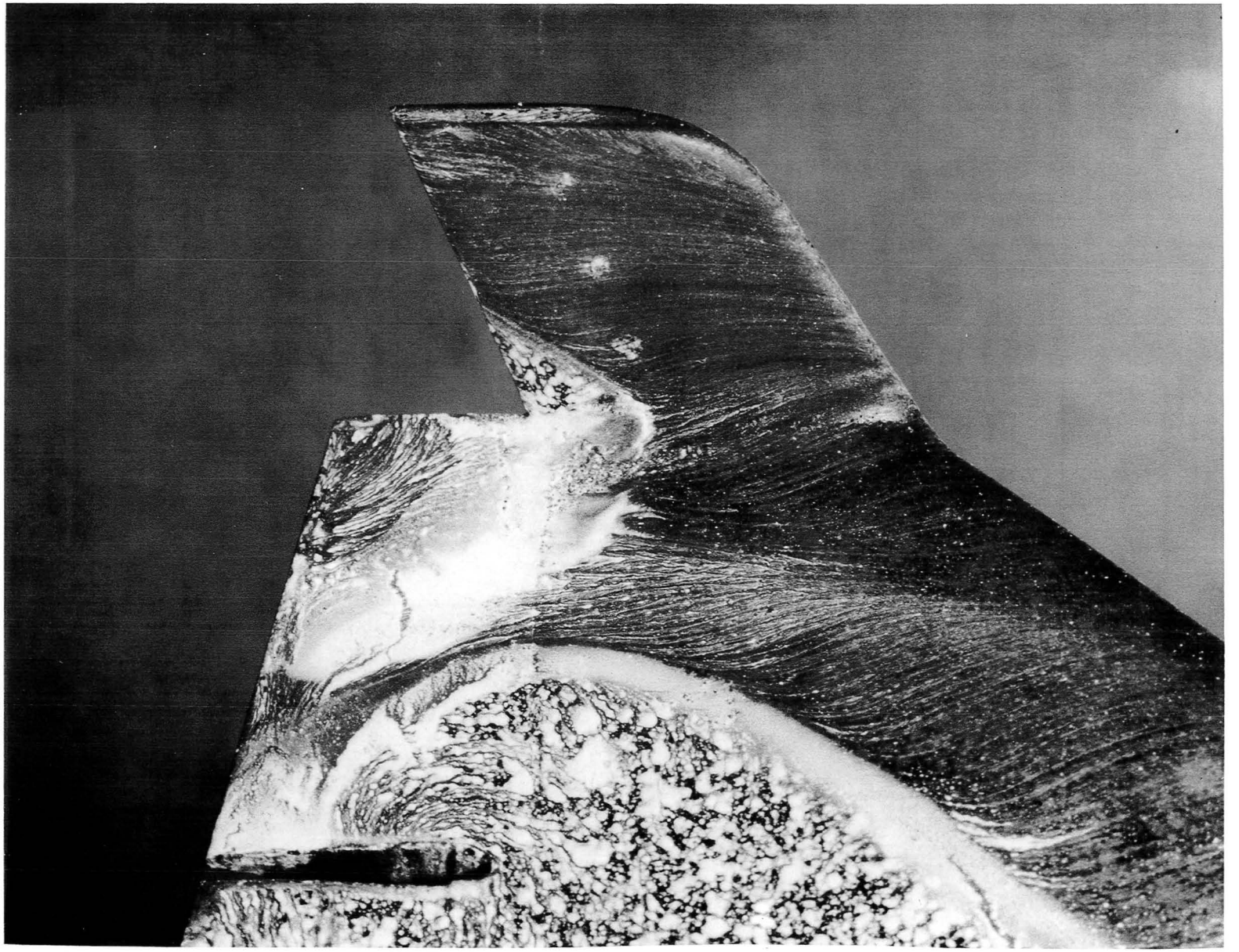

L-84-10,613

(b) Tip-fin inboard surface.

Figure 9. Continued.

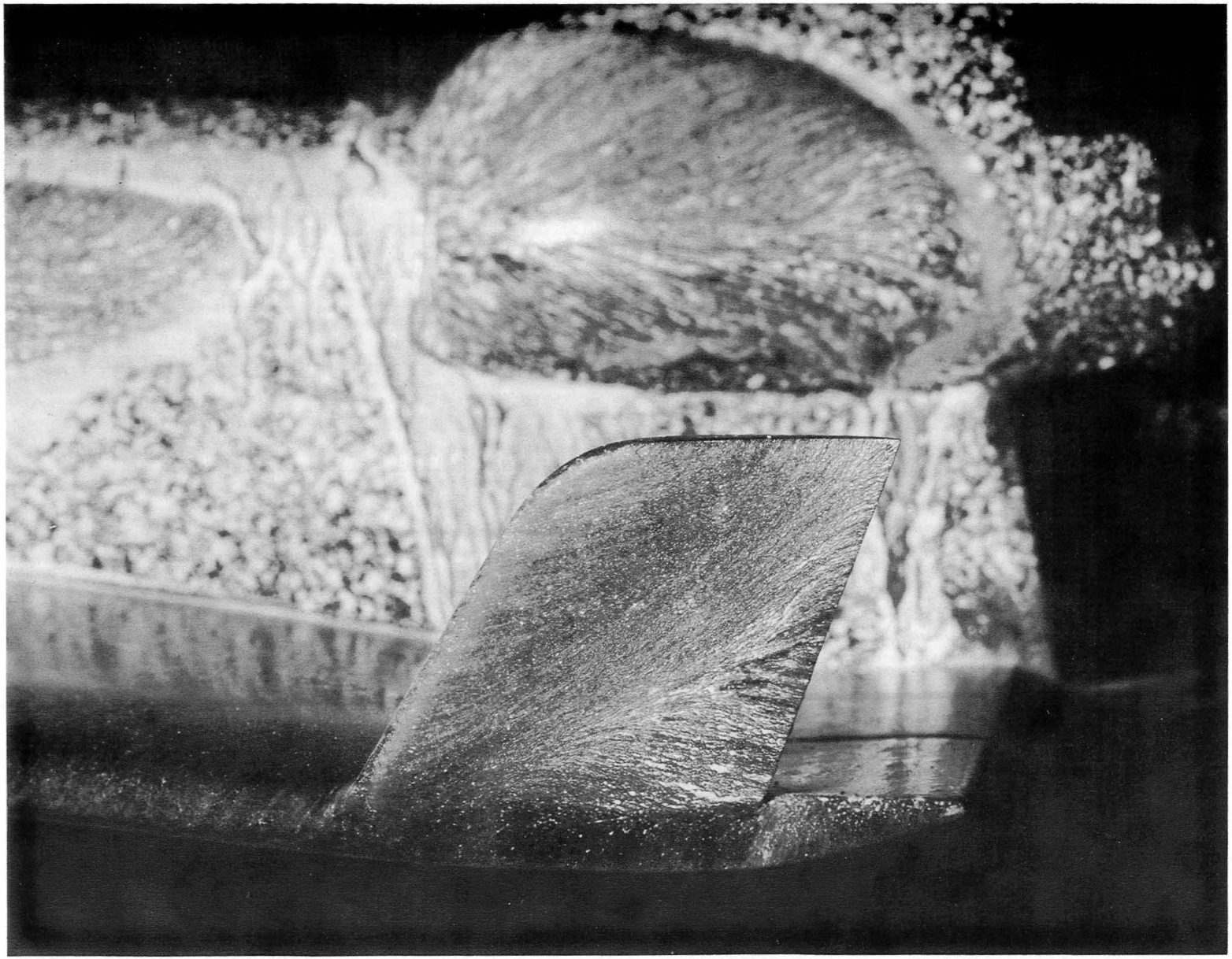

L-84-10,614

(c) Tip-fin outboard surface.

Figure 9. Concluded.

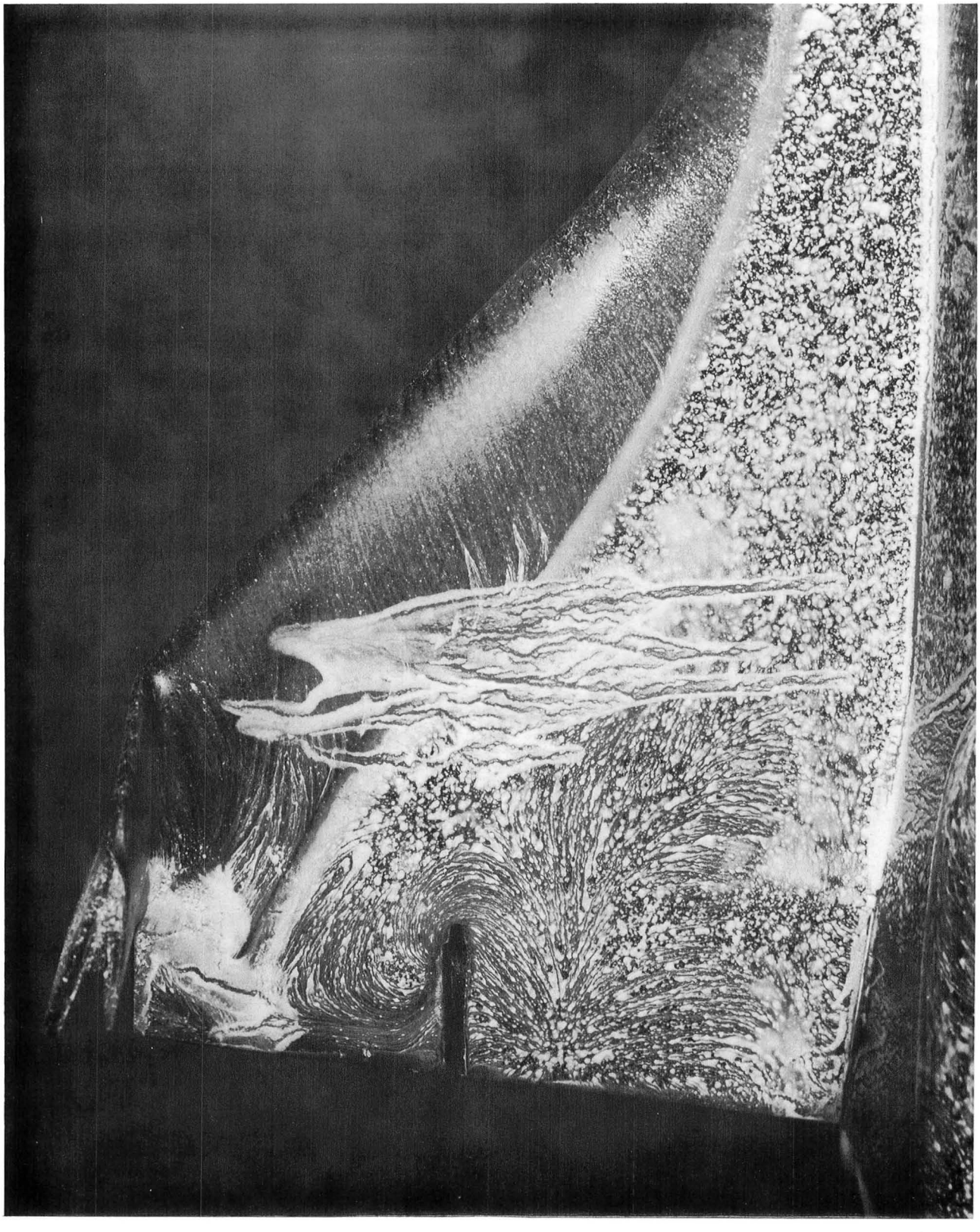

L-84-10,615

(a) Wing leeward surface.

Figure 10. Oil-flow patterns at $\alpha = 30°$ for $\beta = 0°$, $\delta_e = 0°$, and $\delta_{tf} = 20°$.

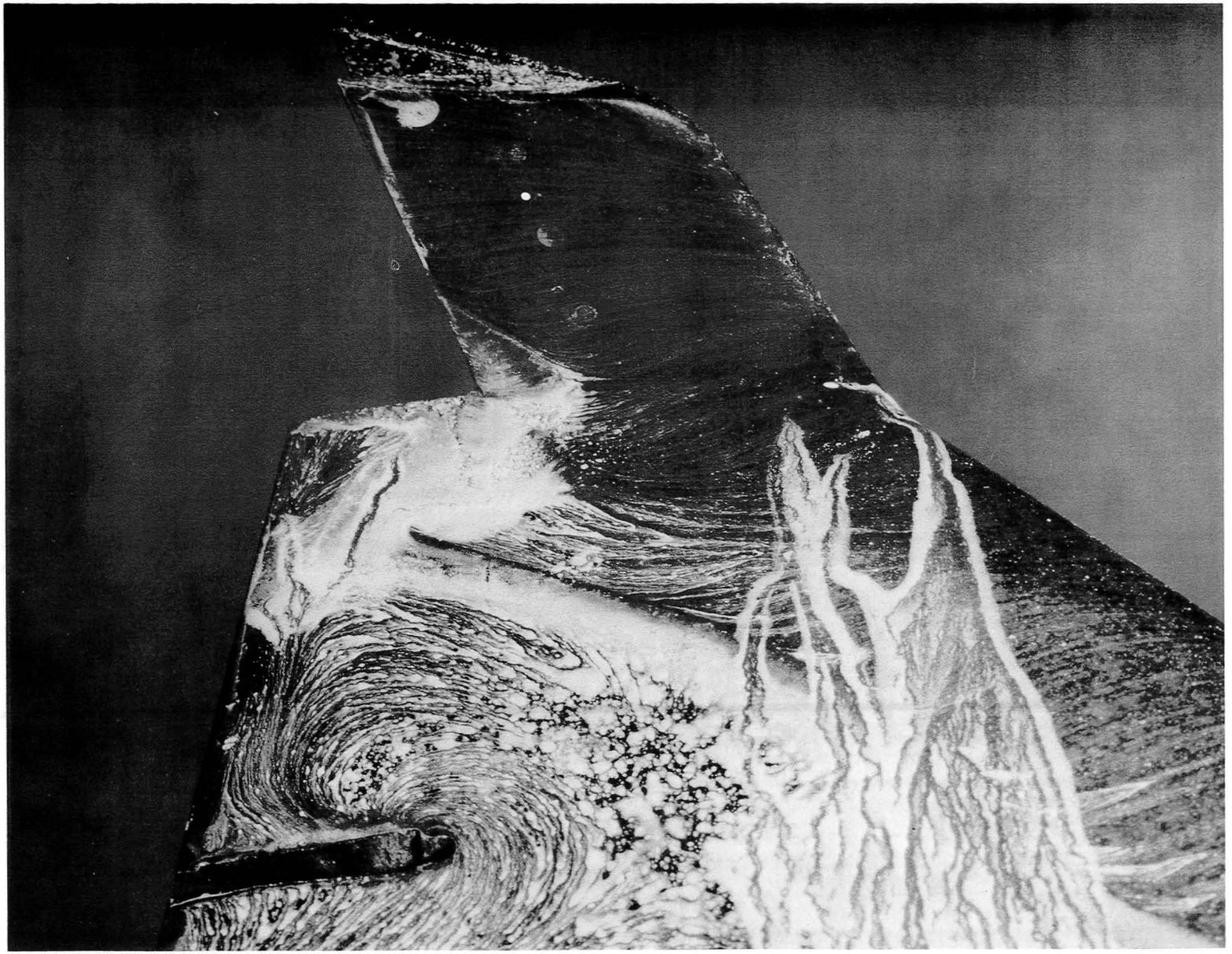

L-84-10,616

(b) Tip-fin inboard surface.

Figure 10. Concluded.

L-84-10,617

(a) Tip-fin outboard surface.

Figure 11. Oil-flow patterns at $\alpha = 20°$ for $\beta = 0°$, $\delta_e = 0°$, and $\delta_{tf} = 20°$.

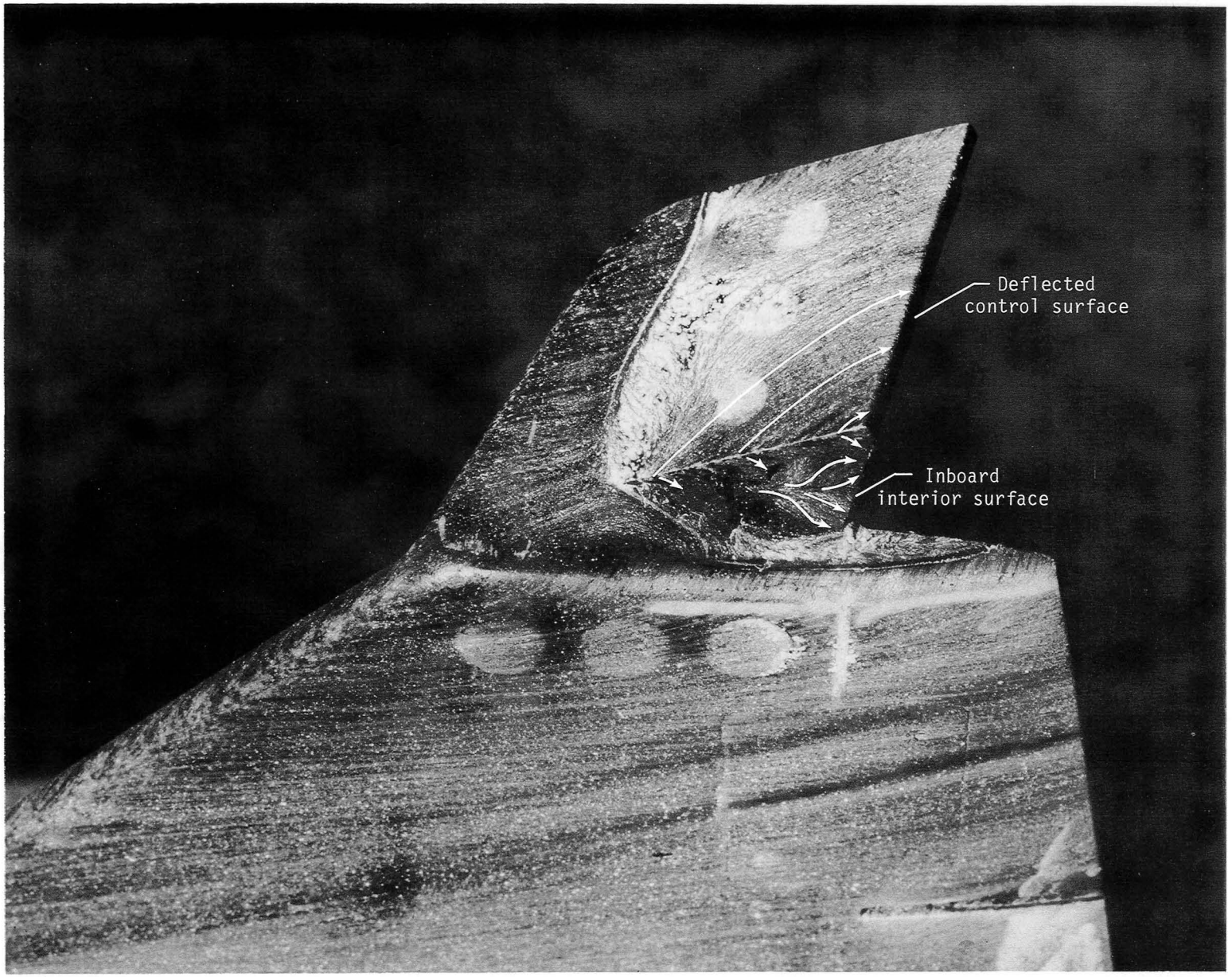

L-84-10,618

(b) Oblique view of tip-fin outer surface.

Figure 11. Continued.

L-84-10,619

(c) Oblique view of tip-fin interior surface.

Figure 11. Concluded.

L-84-10,620

Figure 12. Tip-fin outboard-surface oil-flow patterns at $\alpha = 30°$ for $\beta = 0°$, $\delta_e = 0°$, and $\delta_{tf} = 20°$.

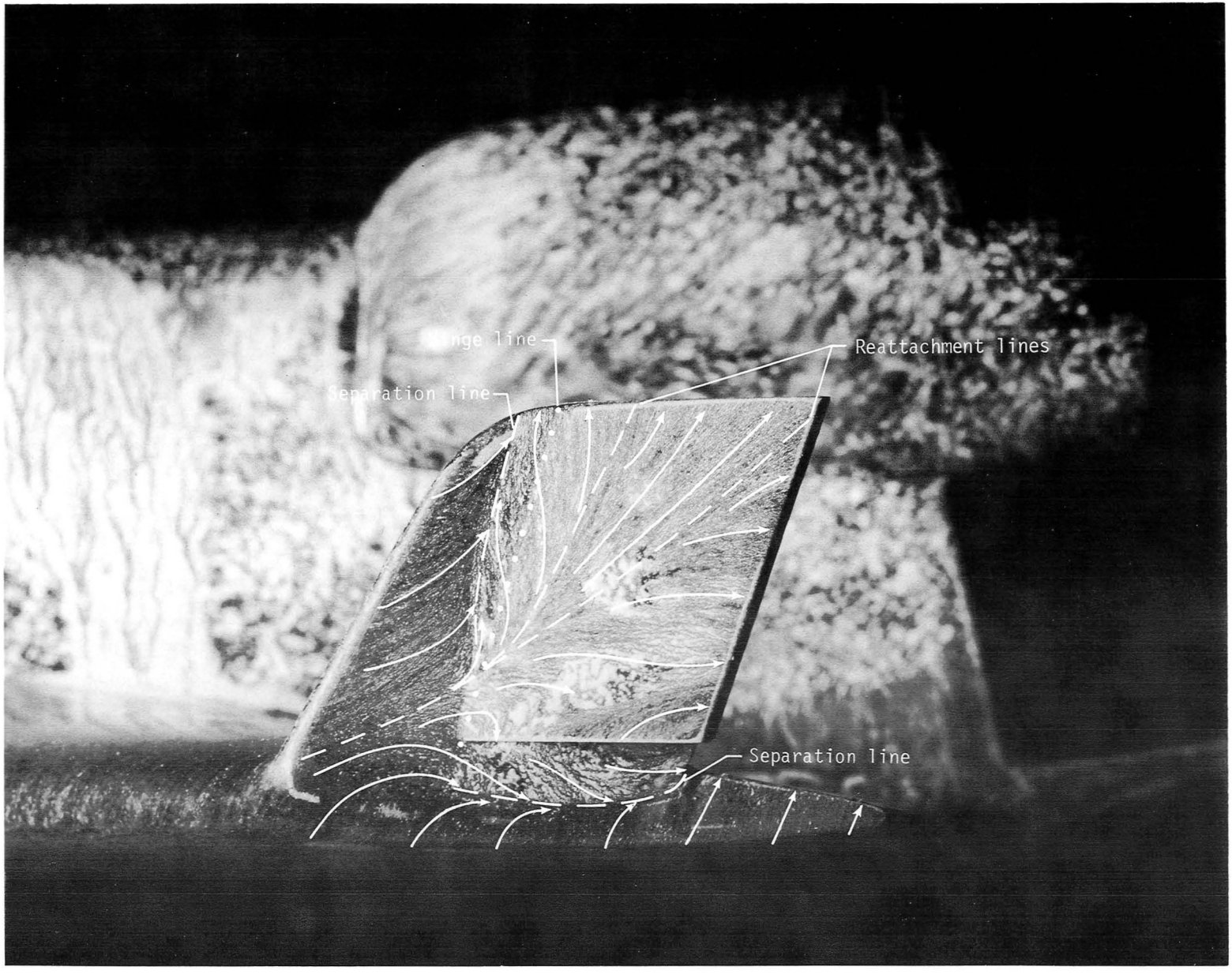

L-84-10,621

Figure 13. Tip-fin outboard-surface oil-flow patterns at $\alpha = 40°$ for $\beta = 0°$, $\delta_e = 0°$, and $\delta_{tf} = 20°$.

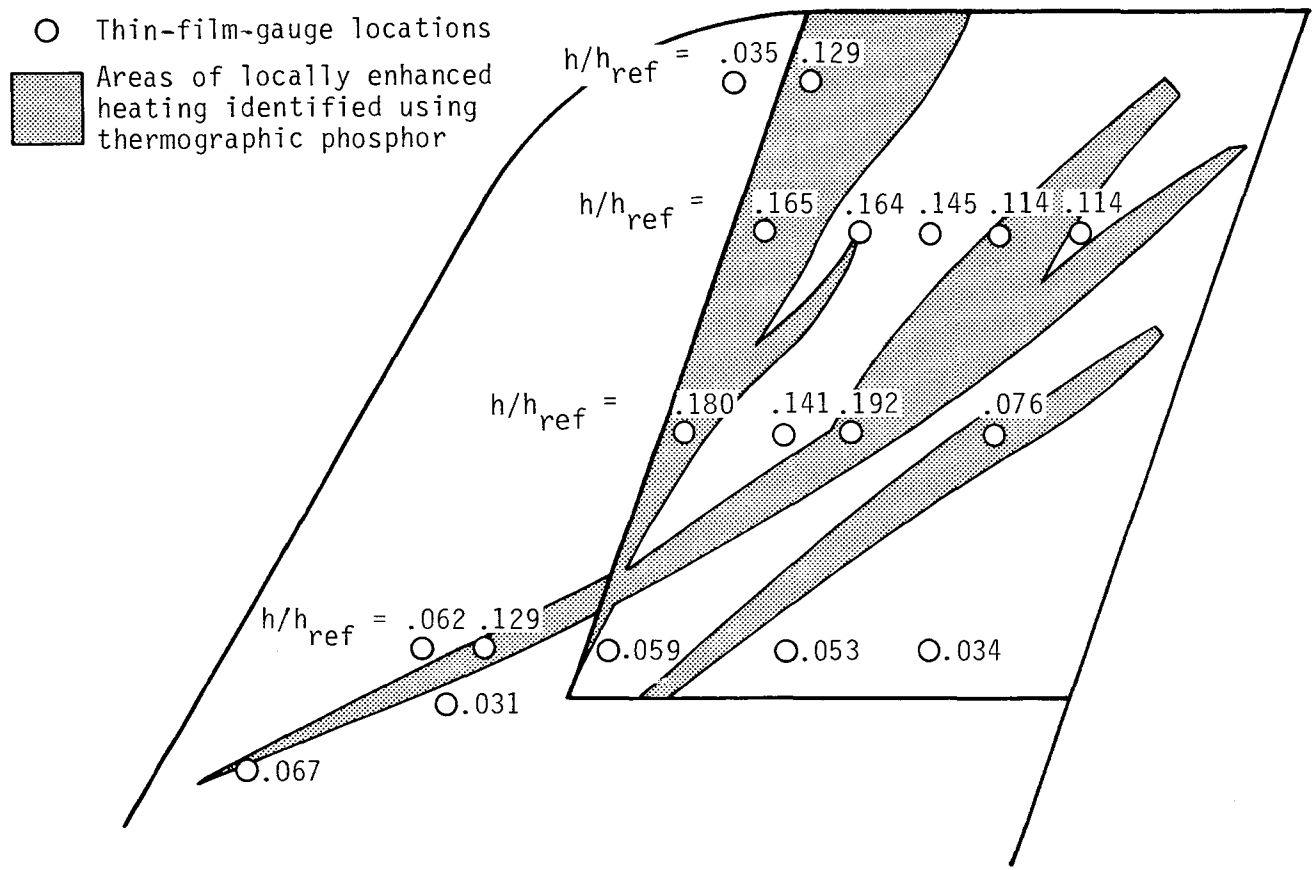

Figure 14. Thermographic-phosphor and thin-film-gauge heat-transfer data for $\alpha = 40°$, $\delta_{tf} = 20°$, $\beta = 0°$, and $M_\infty = 10$.

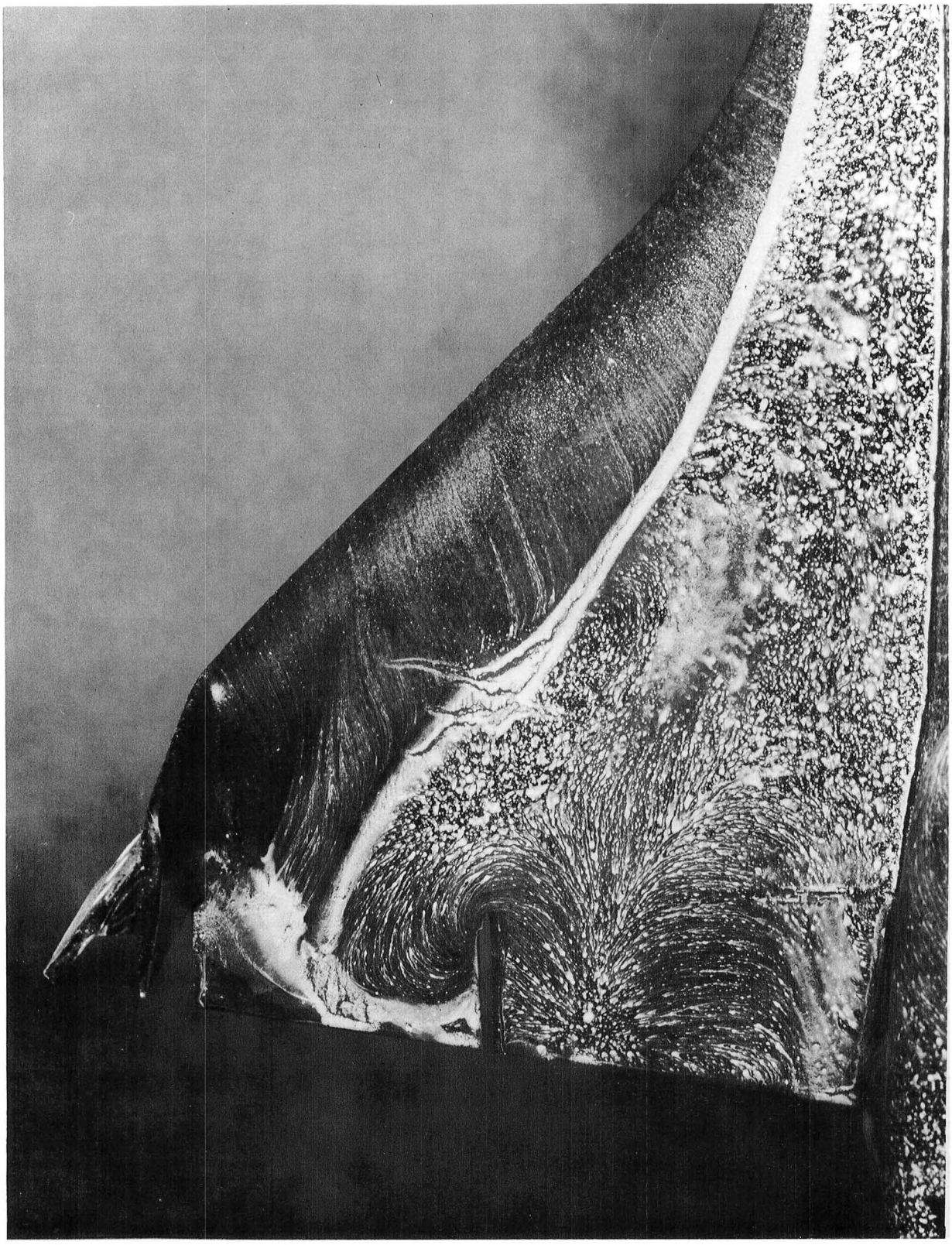

L-84-10,622

(a) Wing leeward surface.

Figure 15. Oil-flow patterns at $\alpha = 30°$ for $\beta = 0°$, $\delta_e = 0°$, and $\delta_{tf} = 40°$.

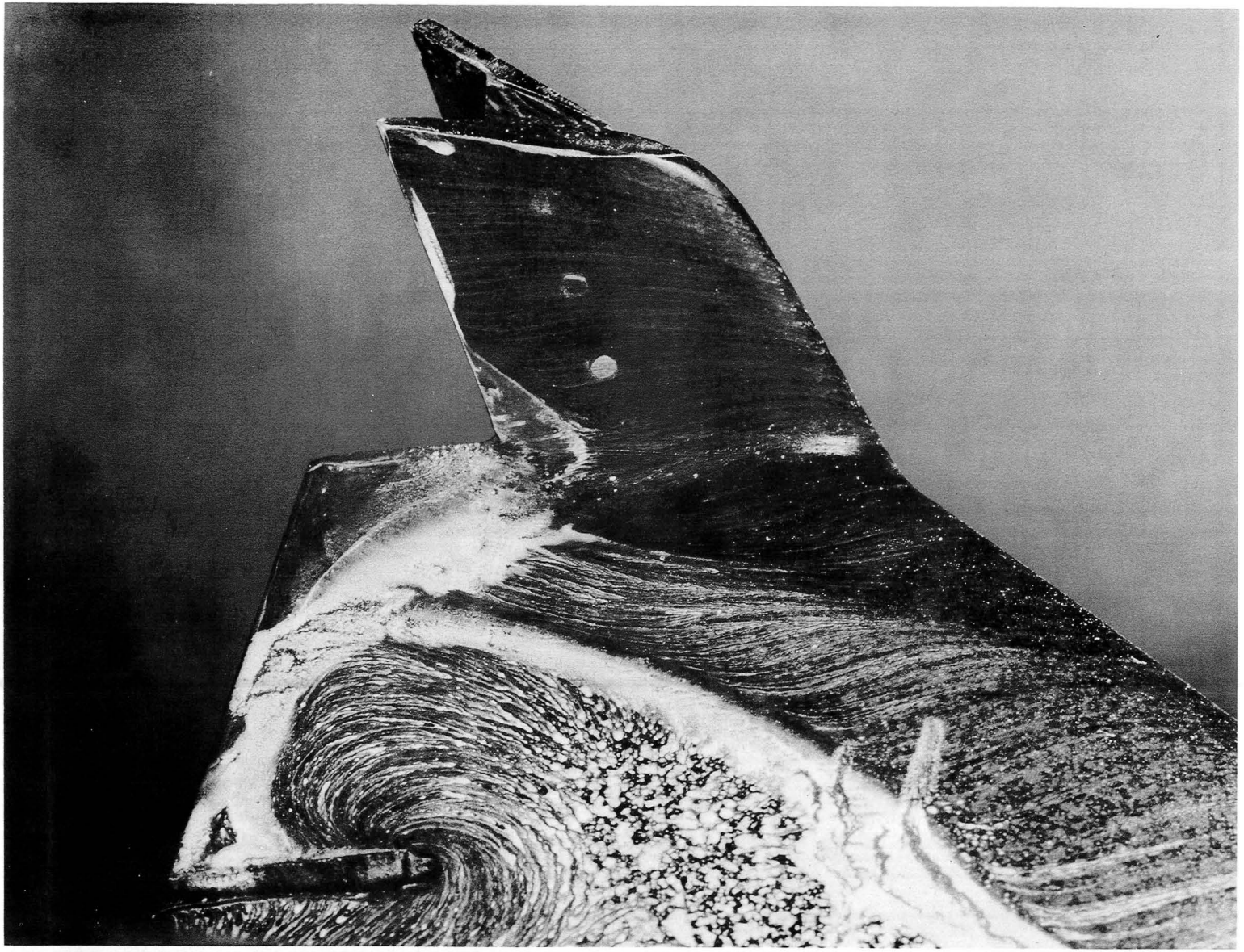

L-84-10,623

(b) Tip-fin inboard surface.

Figure 15. Concluded.

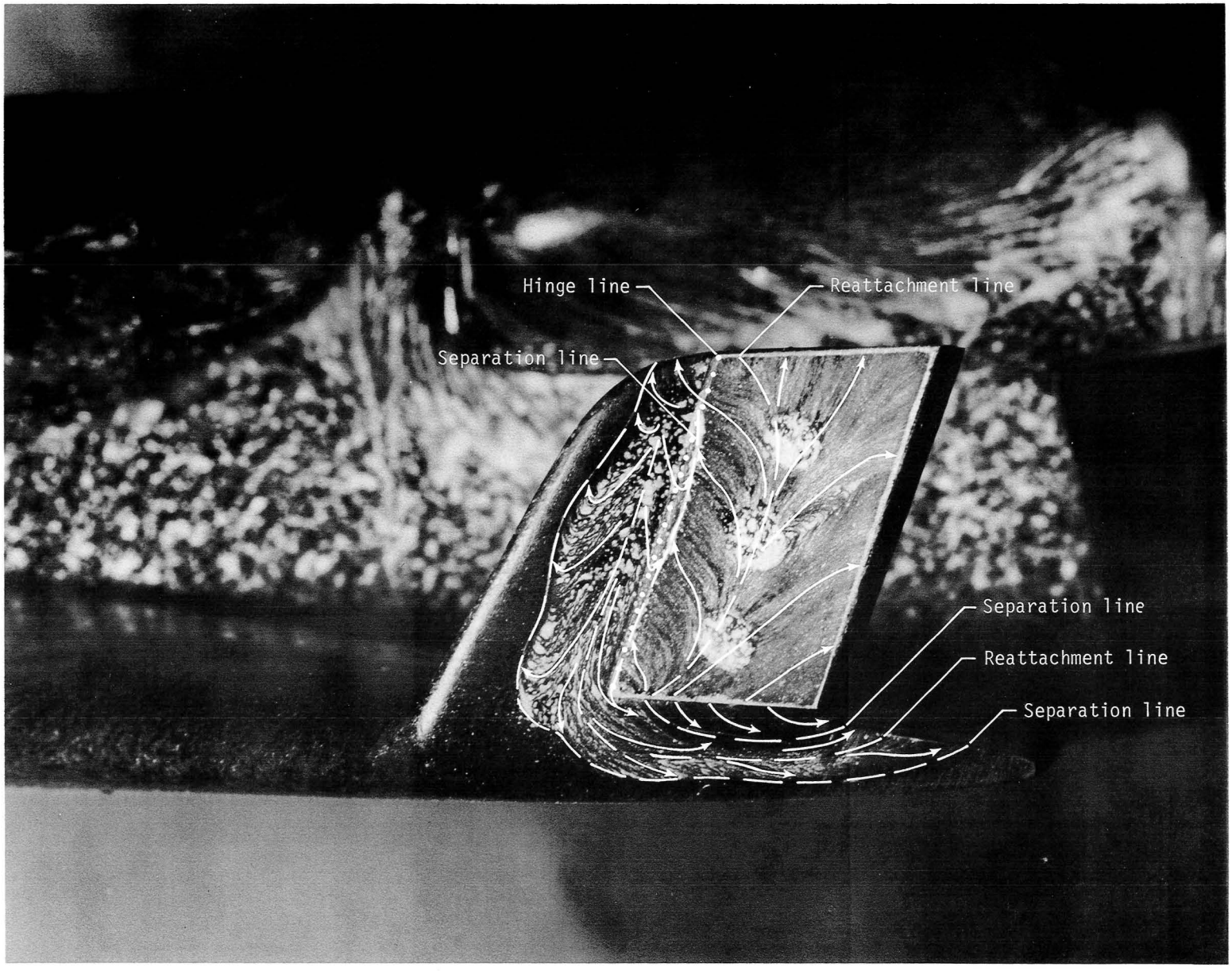

L-84-10,624

(a) Tip-fin outboard surface.

Figure 16. Oil-flow patterns at $\alpha = 20°$ for $\beta = 0°$, $\delta_e = 0°$, and $\delta_{tf} = 40°$.

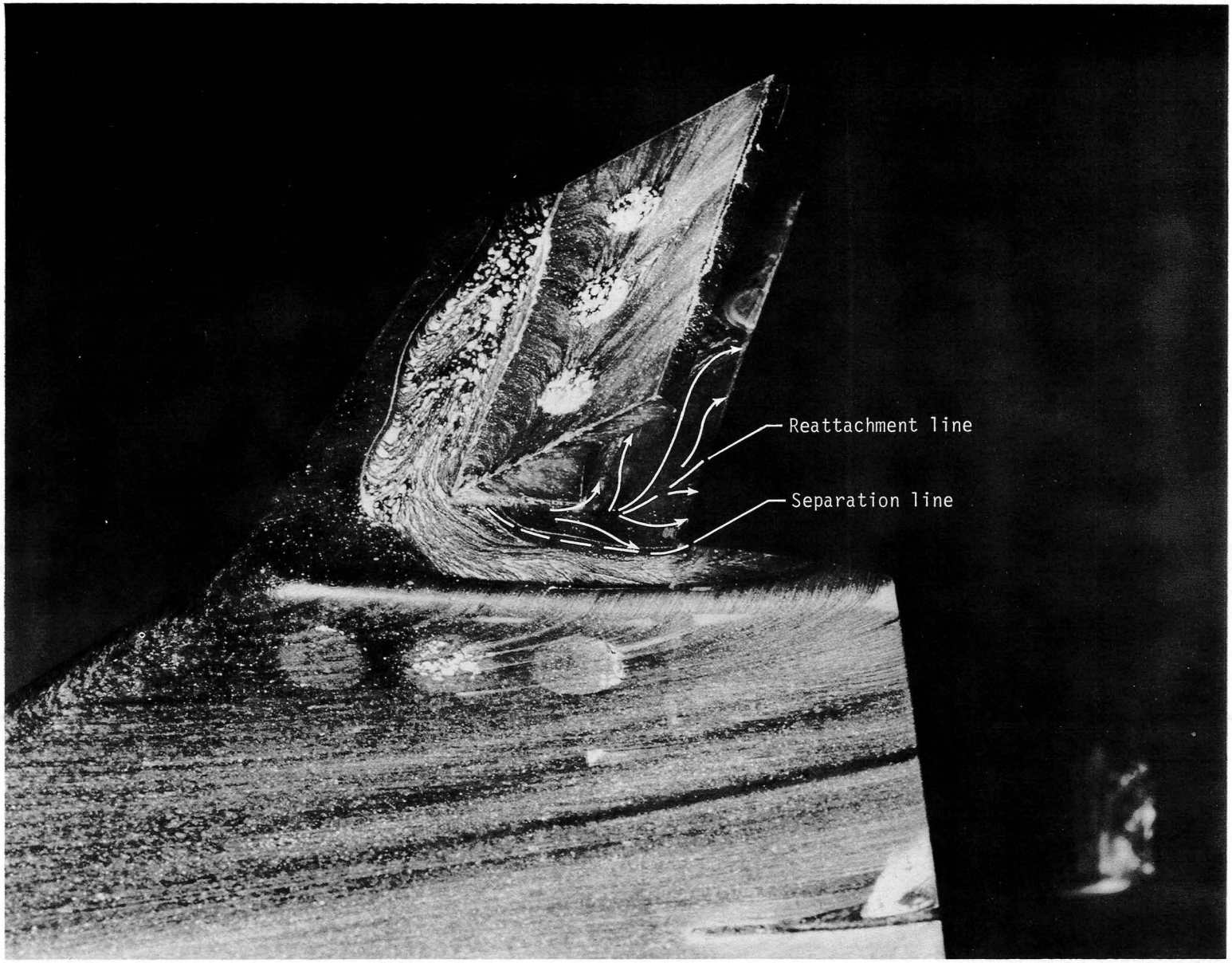

L-84-10,625

(b) Oblique view of tip-fin outboard surface.

Figure 16. Concluded.

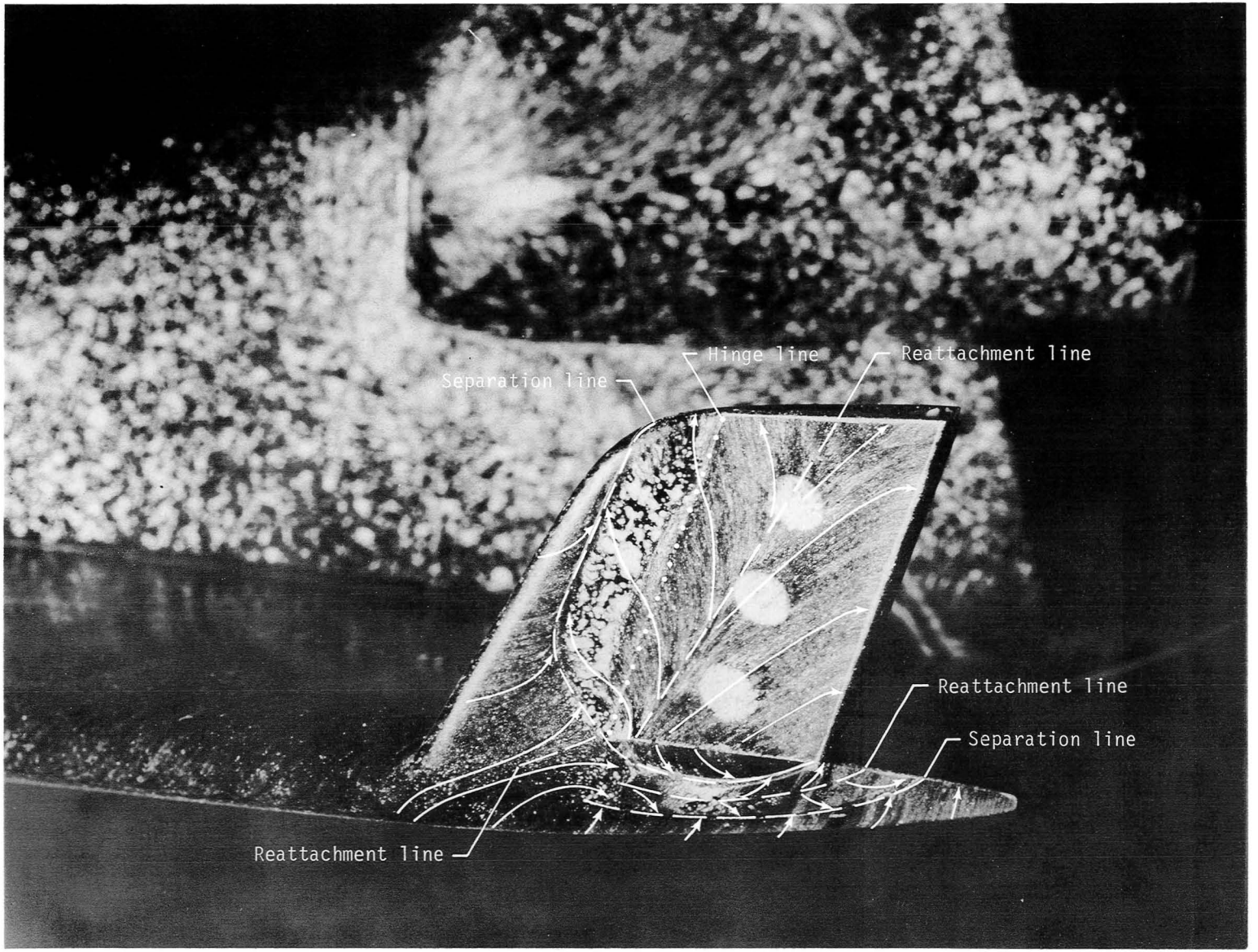

L-84-10,626

Figure 17. Tip-fin outboard-surface oil-flow patterns at $\alpha = 30°$ for $\beta = 0°$, $\delta_e = 0°$, and $\delta_{tf} = 40°$.

L-84-10,627

(a) Tip-fin outboard surface.

Figure 18. Oil-flow patterns at $\alpha = 40°$ for $\beta = 0°$, $\delta_e = 0°$, and $\delta_{tf} = 40°$.

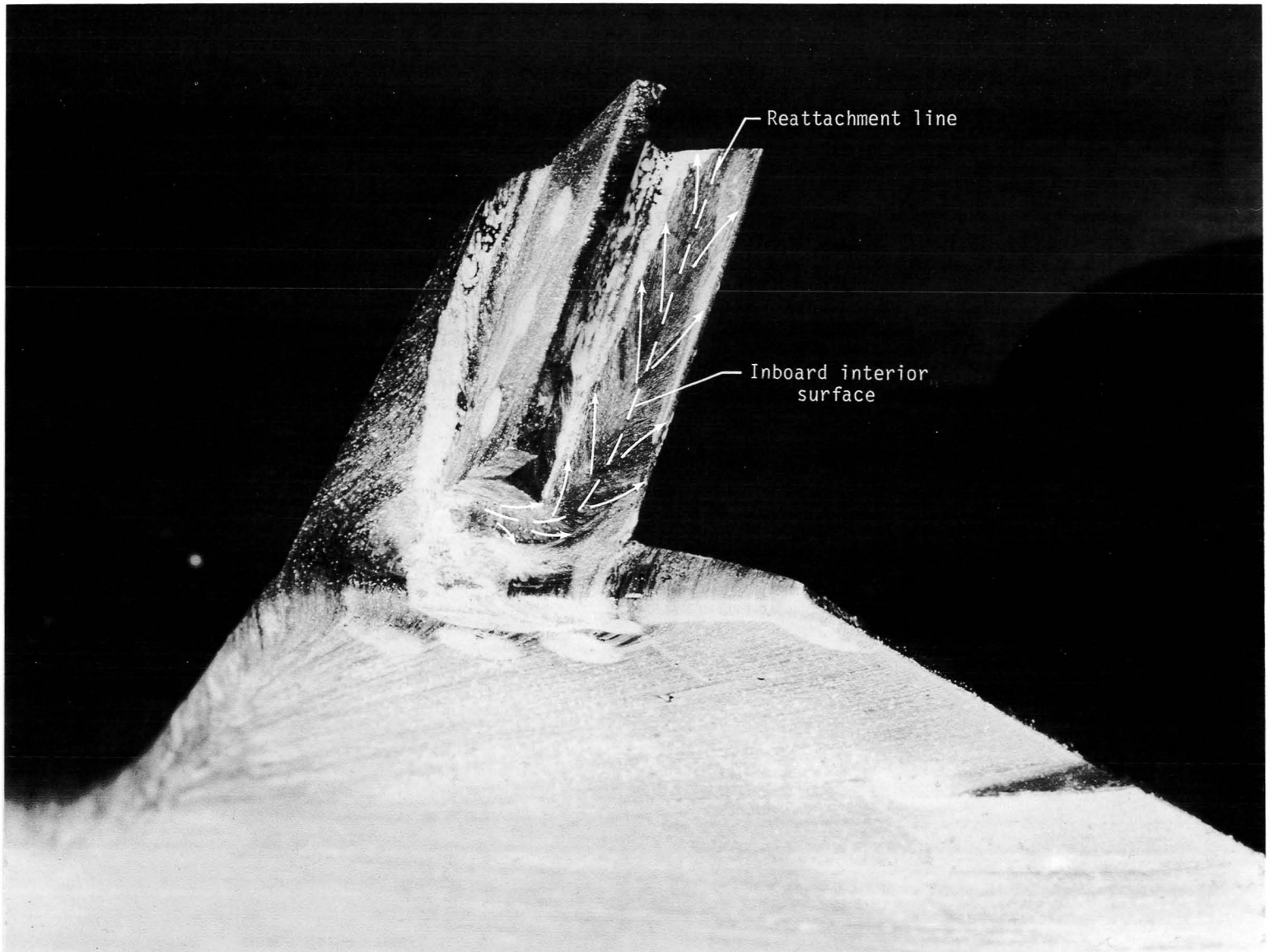

L-84-10,628

(b) Oblique view of tip-fin inboard interior surface.

Figure 18. Continued.

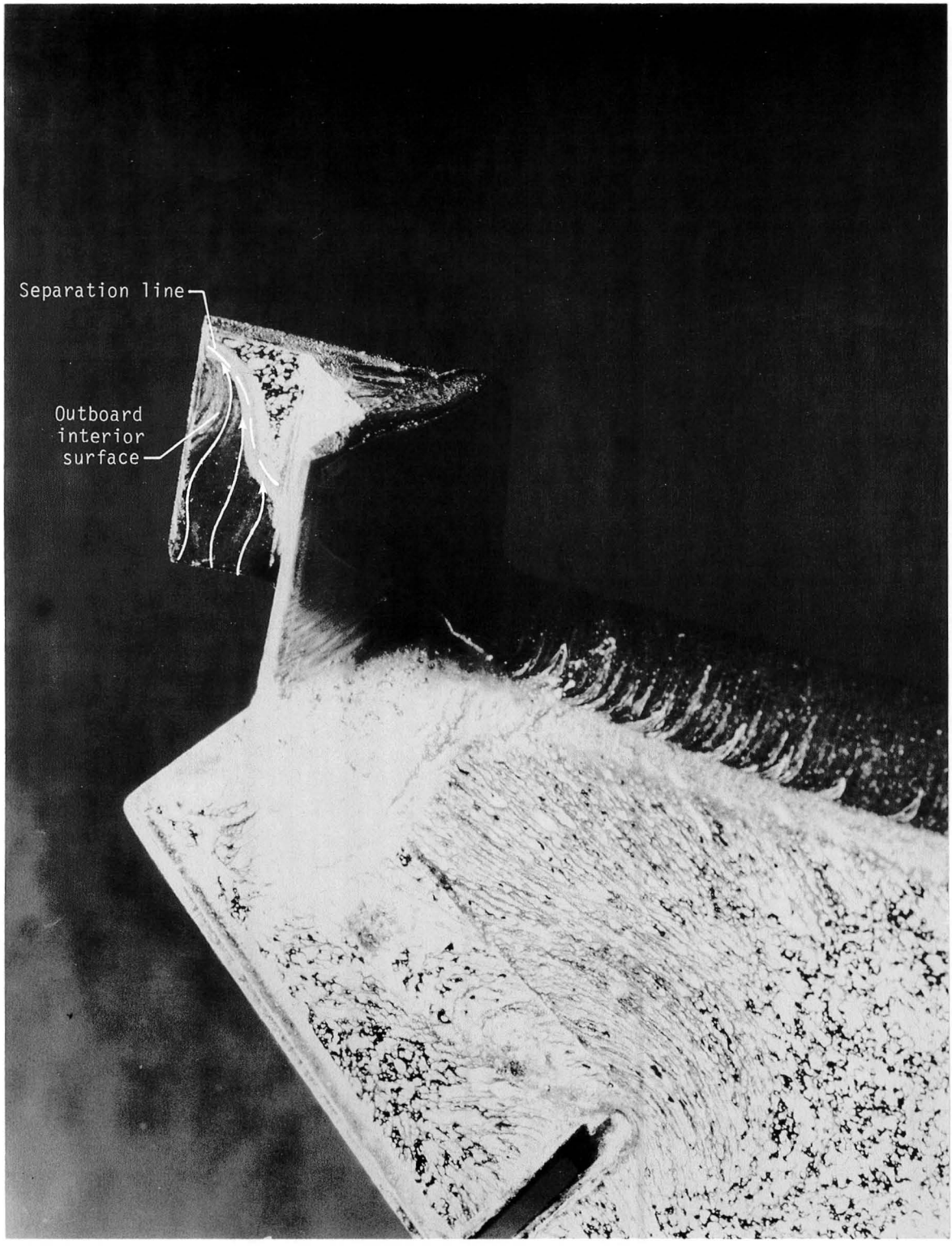

L-84-10,629

(c) Oblique view of tip-fin outboard interior surface.

Figure 18. Concluded.

1. Report No.	2. Government Accession No.	3. Recipient's Catalog No.
NASA TM-86276		

4. Title and Subtitle	5. Report Date
OIL-FLOW STUDY OF A SPACE SHUTTLE ORBITER TIP-FIN CONTROLLER	December 1984
	6. Performing Organization Code: 506-51-13-06
7. Author(s): Vernon T. Helms III	8. Performing Organization Report No.: L-15750
9. Performing Organization Name and Address: NASA Langley Research Center, Hampton, VA 23665	10. Work Unit No.
	11. Contract or Grant No.
12. Sponsoring Agency Name and Address: National Aeronautics and Space Administration, Washington, DC 20546	13. Type of Report and Period Covered: Technical Memorandum
	14. Sponsoring Agency Code

15. Supplementary Notes

16. Abstract

Investigators at the NASA Langley Research Center have examined the possible use of tip-fin controllers instead of a vertical tail on advanced winged entry vehicles. Elimination of the vertical tail and using tip-fins offers the advantages of positive yaw control at high angles of attack and a potential weight savings. The present study used the oil-flow technique to obtain surface flow patterns on a tip-fin installed on a 0.01-scale Space Shuttle orbiter model for the purpose of assessing the extent of flow interference effects on the wing and tip-fin which might lead to serious heating problems. Tests were conducted in air at Mach 10 for a free-stream Reynolds number of 1.13×10^6 at 20°, 30°, and 40° angle of attack and sideslip angles of 0° and 2°. Elevon deflections of −10°, 0°, and 10° and tip-fin control-surface deflections of 0°, 20°, and 40° were employed. Test results were also used to aid in the interpretation of heating data obtained on a Shuttle orbiter tip-fin on another model in a different facility. A limited comparison of oil-flow patterns and heat-transfer data is included in this report. It was determined that elevon deflection angles from −10° to 10° and sideslip angles up to 2° have very little effect on tip-fin surface flow patterns. Also, there is a minimum of interference between the tip-fin and the wing. The most significant flow interactions occur on the tip-fin outboard surface as a result of its control-surface deflections.

17. Key Words (Suggested by Authors(s))	18. Distribution Statement
Tip-fin Oil flow Heat transfer Space Shuttle	Unclassified—Unlimited Subject Category 15

19. Security Classif.(of this report)	20. Security Classif.(of this page)	21. No. of Pages	22. Price
Unclassified	Unclassified	54	A04

For sale by the National Technical Information Service, Springfield, Virginia 22161

NASA-Langley, 1984

National Aeronautics and
Space Administration

Washington, D.C.
20546

Official Business
Penalty for Private Use, $300

THIRD-CLASS BULK RATE

Postage and Fees Paid
National Aeronautics and
Space Administration
NASA-451

NASA

POSTMASTER: If Undeliverable (Section 158
Postal Manual) Do Not Return